Searching for Large Raindrops: A Global Summary of Two-Dimensional Video Disdrometer Observations

PATRICK N. GATLIN

NASA Marshall Space Flight Center, Huntsville, Alabama

MERHALA THURAI AND V. N. BRINGI

Colorado State University, Fort Collins, Colorado

WALTER PETERSEN AND DAVID WOLFF

NASA Goddard Space Flight Center, Wallops Flight Facility, Wallops Island, Virginia

ALI TOKAY

Joint Center for Earth Systems Technology, University of Maryland, Baltimore County, Baltimore, and NASA Goddard Space Flight Center, Greenbelt, Maryland

LAWRENCE CAREY AND MATTHEW WINGO

University of Alabama in Huntsville, Huntsville, Alabama

(Manuscript received 30 March 2014, in final form 5 February 2015)

ABSTRACT

A dataset containing 9637 h of two-dimensional video disdrometer observations consisting of more than 240 million raindrops measured at diverse climatological locations was compiled to help characterize underlying drop size distribution (DSD) assumptions that are essential to make precise retrievals of rainfall using remote sensing platforms. This study concentrates on the tail of the DSD, which largely impacts rainfall retrieval algorithms that utilize radar reflectivity. The maximum raindrop diameter was a median factor of 1.8 larger than the mass-weighted mean diameter and increased with rainfall rate. Only 0.4% of the 1-min DSD spectra were found to contain large raindrops exceeding 5 mm in diameter. Large raindrops were most abundant at the tropical locations, especially in Puerto Rico, and were largely concentrated during the spring, especially at subtropical locations. Giant raindrops exceeding 8 mm in diameter occurred at tropical, subtropical, and high-latitude continental locations. The greatest numbers of giant raindrops were found in the subtropical locations, with the largest being a 9.7-mm raindrop that occurred in northern Oklahoma during the passage of a hail-producing thunderstorm. These results suggest large raindrops are more likely to fall from clouds that contain hail, especially those raindrops exceeding 8 mm in diameter.

1. Introduction

Measurement of the drop size distribution (DSD) enables us to better understand the microphysical processes of precipitating systems, which in turn leads to better parameterization within numerical weather prediction and cloud-resolving models as well as more accurate radar rainfall estimates. Disdrometers have long been used to measure raindrop size and derive empirical relations among integral rainfall parameters (e.g., Fujiwara 1965; Atlas and Ulbrich 1977; Ulbrich 1985; Balakrishnan et al. 1989; Schuur et al. 2001), but the small sampling volume of a disdrometer casts doubt on the representativeness of its measurements at larger spatial scales, especially those on the order of a spaceborne radar sampling volume. Thus empirical relationships derived from disdrometer datasets may introduce error when used in radar retrievals (Chandrasekar and

Corresponding author address: Patrick N. Gatlin, NASA/MSFC ZP11, 320 Sparkman Drive, Huntsville, AL 35805.
E-mail: patrick.gatlin@nasa.gov

DOI: 10.1175/JAMC-D-14-0089.1

© 2015 American Meteorological Society

Bringi 1987; Smith et al. 1993; Jaffrain and Berne 2012). These issues have motivated recent studies on the small-scale variability of the DSD (e.g., Miriovsky et al. 2004; Lee et al. 2009; Tokay and Bashor 2010; Tapiador et al. 2010; Jaffrain et al. 2011). As such, a network of disdrometers has been employed by NASA's Global Precipitation Measurement (GPM) mission Ground Validation (GV) efforts to construct a database of DSD characteristics and derive relationships among DSD parameters that may be used to develop and refine precipitation retrieval algorithms for the GPM *Core Observatory* satellite (Hou et al. 2014).

Quantitative precipitation estimation (QPE) with weather radar often involves integral rainfall parameters, such as rainfall rate and reflectivity. Following Ulbrich (1985), any integral rainfall parameter can be expressed as the Pth moment of the DSD by

$$P = a_P \int_{D_{\min}}^{D_{\max}} D^P N(D)\, dD, \qquad (1)$$

where $N(D)$ is the number of drops of diameter D in the size interval dD, a_P is a constant, and $D_{\min}$ and $D_{\max}$ are the size limits of integration, which depend upon the measuring device. Employing an assumption that the measured DSD extends over an infinite size range (i.e., untruncated) introduces error in calculated integral rainfall parameters (Ulbrich 1985) and empirical relationships used for radar retrieval of rainfall (Ulbrich 1992) or DSD parameters (Ulbrich and Atlas 1998). The DSD moments, especially the higher-order ones like radar reflectivity, which is related to the sixth moment, are significantly influenced by truncation at $D_{\max}$ (Ulbrich and Atlas 1998). An overestimation of $D_{\max}$ can lead to overestimation of (1), which in turn can detrimentally impact derived empirical relationships used for radar retrievals of rainfall and water content.

Furthermore, the type of model employed to describe the DSD may not accurately depict the tail of the drop size spectrum. Both the modified gamma (Ulbrich 1983) and Marshall–Palmer (Marshall and Palmer 1948) distributions often underestimate the concentration of large raindrops (Zrnić et al. 2000). Thus the presence of large drops may require employing a more complex model, such as the bi-exponential form (e.g., Schuur et al. 2001), to describe the observed DSD. To substantiate the use of such complex DSD models as well as refine them, it is important for us to gain a better understanding of the actual concentration of large raindrops.

The probability of recording large raindrops with a disdrometer is limited, largely because of sampling issues (Smith et al. 1993). Although radar has a significantly larger measurement volume and thus has a better chance of sampling $D_{\max}$, it does not provide a direct measure of raindrop diameter. Dual-polarimetric radar does provide a measure of drop shape and thus size via drop shape–size relations (e.g., Beard and Chuang 1987; Brandes et al. 2002; Thurai et al. 2007), but all the raindrops contribute to the measurement, especially the larger ones, which makes it difficult to estimate the size of the single largest raindrop in the radar resolution volume. An empirical relation can be devised to estimate $D_{\max}$ as a function of reflectivity, but because of difficulty in estimating the size of a single raindrop from a reflectivity-weighted measurement, adjustment factors have been used (e.g., Brandes et al. 2003), which can introduce large errors into the estimate. The lack of knowledge about $D_{\max}$ has required an assumption to be made in the calculation of (1), for example, in radar-scattering simulations. Many calculate $D_{\max}$ as a function of D_m or D_0, where D_m and D_0 are the mass-weighted mean diameter and median volume diameter, respectively (e.g., Smith et al. 1993; Keenan et al. 2001; Gorgucci et al. 2002; Bringi et al. 2002). Whereas others have assigned a constant value to $D_{\max}$, for example, 8 mm is often used (e.g., Sachidananda and Zrnić 1987; Balakrishnan et al. 1989; Illingworth and Caylor 1989; Carey et al. 2000). The value of $D_{\max}$ employed in deriving radar–rainfall relationships can produce significantly different results (Keenan et al. 2001), and the presence of large raindrops greatly influences radar signal attenuation, especially at C-band frequencies (Zrnić et al. 2000; Carey et al. 2000; Keenan et al. 2001; Carey and Petersen 2015). One way to increase our confidence in $D_{\max}$ assumptions as well as improve our knowledge of large raindrop concentrations is to examine long-term measurements from *well-calibrated* disdrometers that sample a variety of precipitation regimes.

This study has compiled and analyzed one of the *largest and geographically diverse* sets of two-dimensional video disdrometer (2DVD) data discussed in the literature to date. The 2DVDs included in this dataset were deployed over the past decade in various locations around the globe (Table 1). We examine this large dataset to do the following: 1) find when and where the largest raindrops occur, 2) provide some observational evidence to validate common assumptions about the tail of the DSD, and 3) provide insight about the source of large raindrops. A description of the dataset and filtering techniques to remove nonrain are provided in the next section and appendix. Section 3 provides the results of this study, which includes an examination of seasonal and diurnal trends of large raindrop occurrence as well as $D_{\max}$–D_m statistics. A discussion of these results in light of the three objectives listed above is provided in section 4. A summary of this study and concluding remarks are given in the final section.

TABLE 1. Overview of the 2DVD datasets included in this study.

2DVD location (field campaign)	No. of 2DVDs (proprietor)	Dates of operation	No. of 1-min DSD spectra
Florida (TEFLUN-B)	2 (University of Iowa; NASA)	June 1998–August 1998	2857
Amazon basin (TRMM-LBA)	2 (University of Iowa; NASA)	January 1999–February 1999	2237
Hiratsuka, Japan*	1 (CSU)	July 2003–November 2003	29 560
Okinawa, Japan	1 (CSU)	November 2003–June 2004	24 415
Puerto Rico*	1 (CSU)	August 2004–February 2006	37 724
Colorado*	1 (CSU)	June 2004–August 2004, February 2006–October 2006	13 841
Ontario [*CALIPSO* Validation Project (C3VP); GPM Cold Season Precipitation Experiment (GCPEx)]	6 (CSU; NASA)	November 2006–July 2007, October 2011–March 2012	18 528
Huntsville, AL	6 (CSU; NASA)	July 2007–present	204 070
Southern Finland (LPVEx)	3 (NASA)	September 2010–January 2011	8653
Oklahoma [Midlatitude Continental Convective Clouds Experiment (MC3E); ARM]	7 (NASA; DOE)	April 2011–December 2013	66 663
Southern France [Hydrological Cycle in the Mediterranean Experiment (HyMeX)]	1 (NASA)	September 2012–November 2012	1995
Rome, Italy (HyMeX)	1 (NASA)	September 2012–November 2012	6433
Iowa [Iowa Flood Studies (IFloodS)]	6 (NASA)	April 2013–June 2013	53 969
Wallops Island, VA	6 (NASA)	May 2012–March 2013, July 2013–December 2013	55 249
Darwin, Australia (ARM)	1 (DOE)	February 2011–December 2013	70 773
Manus Island, Papua New Guinea (ARM)	1 (DOE)	December 2011–December 2013	98 988
Gan Island, Maldives [ARM MJO Investigation Experiment (AMIE)]	1 (DOE)	October 2011–February 2012	11 798
Koto Tabang, West Sumatra, Indonesia	1 (Shimane University)	November 2005–April 2007	67 911

* Data collected by one 2DVD but at different sites for this location.

2. Dataset description and analysis techniques

The 2DVD has been shown to provide DSD measurements that are in good agreement with other types of disdrometers (e.g., Tokay et al. 2001, 2002, 2013; Miriovsky et al. 2004; Thurai et al. 2007). However, the capability of the 2DVD to accurately measure raindrops at the larger diameter end of the size spectrum makes this instrument well suited for large raindrop studies. Although a detailed discussion of the 2DVD and its evolution is given in other works (e.g., Kruger and Krajewski 2002; Schönhuber et al. 2008), we provide a brief overview of its principles of operation next.

a. Overview of 2DVD

The 2DVD is an optical-type disdrometer that measures objects as they pass through two orthogonal planes of light that are vertically displaced by 6–7 mm (Fig. 1). This vertical separation enables a direct measure of particle fall speed. Each optical plane consists of a light source and a line scan camera that scans the measurement area every 18 μs "looking" for obstructions to the light source. The nominal measurement area, which is 10 cm × 10 cm and centered in the middle of the 25 cm × 25 cm 2DVD inlet, has been optimized to mitigate contamination from raindrop splashing. The maximum number of line scan pixels shadowed by a raindrop corresponds to the width of that raindrop. Since both the fall velocity and width of the raindrop are measured, the ratio of the minor to major axes of the raindrop may be estimated. The raindrop detected by each camera can then be matched to provide a reconstruction of the drop shape. The 2DVD has a nominal resolution of 0.2 mm, and its large measurement area enables it to measure the

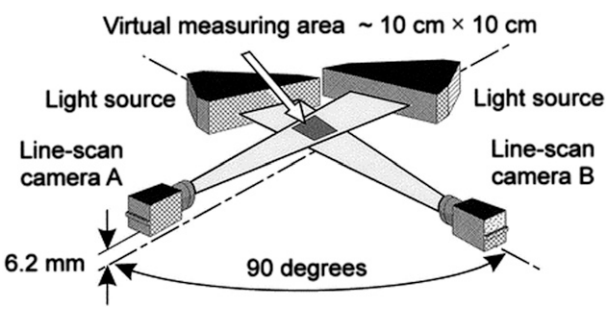

FIG. 1. 2DVD principles of operation (adapted from Kruger and Krajewski 2002).

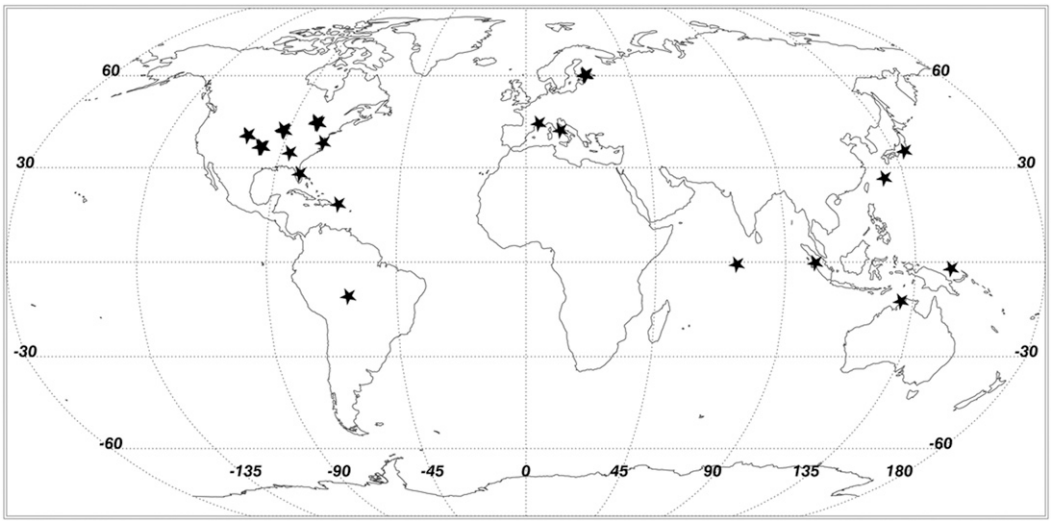

FIG. 2. Locations of the 2DVDs used to construct the raindrop dataset presented in this study.

largest of naturally occurring raindrops. Routine calibration of the 2DVD is performed by dropping metal spheres of known diameters (ranging from 0.5 to 10 mm) through the measurement area to ensure the instrument detects and records the correct-sized objects. This calibration also allows for the vertical distance between the optical planes to be precisely measured, thereby ensuring accurate fall speed measurements. The 2DVD is one of the few disdrometers currently available that allows exact calibration of the instrument to be *readily* performed in the field.

b. 2DVD deployments

The data used in this study were collected using all three generations of the 2DVD (Schönhuber et al. 2008). Although the first generation 2DVD is subject to measurement errors because of its tall profile, these self-induced wind effects mainly affect the smaller raindrop end of the size spectrum (Nešpor et al. 2000). The dataset is composed of 2DVD measurements from numerous locations around the globe (Fig. 2). An overview of these deployment locations, including periods of operation and number of rainy minutes, is provided in Table 1. Some of the data collected by these 2DVDs have been used in numerous other studies (e.g., Tokay et al. 2001, 2002, 2013; Bringi et al. 2003, 2006; Maeso et al. 2005; Kozu et al. 2005; Thurai and Bringi 2008; Thurai et al. 2012, 2013; Williams et al. 2014), but, until now, *there has yet to be a such a large and diverse set of 2DVD measurements compiled*.

c. Data filtering

Large raindrops will be defined in this study as having equivalent spherical diameters D_{eq} of 5 mm or greater and giant raindrops are defined as those with $D_{eq} \geq 8$ mm. Since this study is concerned with finding large raindrops, some filtering of the dataset has been performed to remove snowflakes, hail, and other nonrain objects (e.g., insects, calibration spheres). Nearby temperature data from automated surface stations were used in an attempt to remove 2DVD measurements that may contain snow, sleet, or freezing rain. If the minimum hourly temperature was below 3°C, it was removed from further consideration. As a result, about 12% of the 2DVD measurements between the dates in Table 1 were excluded from further consideration. Also, the diameters of objects considered were limited to $0.2 \leq D_{eq} \leq 12$ mm. This accounts for the instrument resolution and reduces the chance that hail or some other large, nonrain particle (e.g., the occasional insect was found in some raw 2DVD camera "images") is included in our final dataset. This maximum diameter threshold was somewhat arbitrarily chosen, but it is large enough to ensure we did not remove the largest raindrops possible and small enough to remove the occasional unwanted giant object. Only 5% of the objects recorded by the 2DVDs fell outside these diameter limits.

Although the vast majority of the snowflakes contained within the initial 2DVD dataset (i.e., unfiltered) were removed by this 3°C filter, it is possible that some snowflakes may have occurred at slightly warmer temperatures. Also, partially melted graupel and small hail may have been sampled during some rain events. Thus, in a similar fashion to a few other 2DVD studies (e.g., Kruger and Krajewski 2002; Tokay et al. 2001; Thurai and Bringi 2005), a velocity filter was applied, which made the distinction between snow/graupel and rain much more straightforward, especially for $D_{eq} \geq 5.0$ mm.

Since there is some uncertainty about the terminal velocity of raindrops exceeding 5–6 mm (see discussion in appendix), we employed another filter based on the 2DVD measurements of axis ratio. Thus experimental axis ratio measurements in the Mainz wind tunnel (Thurai et al. 2009; Szakáll et al. 2010) and those observed with the 2DVD during an 80-m bridge experiment (Thurai and Bringi 2005) were utilized to remove nonrain objects. Although technicians try their best to ensure calibration datasets are kept separate from precipitation datasets, calibration spheres have been found to exist in some of these datasets (see circled regions around diameters of 3–10 mm in Figs. A1a,b). Fortunately the calibration spheres are easily identifiable because their major and minor axes are equivalent and these spheres only occur in the datasets during precipitation-free periods. This axis ratio filter roughly follows the boundaries given in Fig. 2 of Thurai et al. (2009). Additional details of the velocity and axis ratio filtering and its application to this dataset are provided in the appendix. The velocity and axis ratio filter removed 32% of the objects measured by the 2DVD within the diameter limits we considered, including 71% of the objects exceeding 5.0 mm.

3. Results

a. Rainfall summary

After filtering the dataset, just over 240 million objects recorded by the 2DVDs were classified as raindrops. Collectively they resulted in 998 cm of rainfall accumulation over the course of 2595 rainy days (i.e., days with at least 0.1 mm of rainfall accumulation). Roughly 75% of the 5-mm or larger objects recorded by the 2DVD were removed during the filtering process (Fig. A1e, below), leaving only 10 493 large raindrops. The 2DVD measurements in Huntsville, Alabama, mostly with the Colorado State University (CSU) low-profile 2DVD, constituted 25% of the raindrop dataset including 2938 large raindrops. This comes as no surprise considering a 2DVD has been recording raindrops at this same location for more than 5 years (Table 1).

To compare the frequency of large raindrop observations from the 18 locations listed in Table 1, the sampling bias must be removed. The number and duration of 2DVDs deployed can bias the results at each location. For example, the Oklahoma dataset consists of 66 663 min of raindrop spectra, which were obtained over the course of several years and includes seven 2DVDs concentrated in a 5 km^2 area during the spring of 2013, whereas the dataset collected in Rome over three months with one 2DVD consisted of only 6433 min of raindrop spectra (Table 1). Thus we considered the fraction of 1-min raindrop spectra that contained large raindrops. A spectrum that had at least one large raindrop was defined as a large raindrop spectrum. We also wanted to determine where the most large raindrops were sampled in each spectrum, which may provide some insight into the efficiency of large raindrop production. Thus we also considered the normalized number of large raindrops sampled at each location, where the total number of large raindrop spectra sampled at each location was used as the normalization factor (i.e., we divided the total number of large raindrops by the total number of large raindrop spectra).

Only 0.4% of the 775 664 one-min raindrop spectra sampled consisted of large raindrops. Although the most 1-min raindrop spectra were sampled in Huntsville (Table 1), Puerto Rico had the greatest percentage of large raindrop spectra (Fig. 3). About 1.1% of the 37 724 one-minute raindrop spectra sampled in Puerto Rico contained a total of 1489 large raindrops. This is a considerably higher percentage than that sampled at any of the other 17 locations. Eight of the other locations, including Oklahoma and Darwin, were within an order of magnitude of the relative sampling of large raindrop spectra in Puerto Rico. The fewest number of raindrop spectra containing large raindrops was in Hiratsuka, Japan, despite 29 560 min of rain being sampled here. This is in contrast to the 11 995 min of rain sampled in the Maldives, which consisted of a higher percentage of large raindrop spectra than Hiratsuka even though both locations had a 2DVD deployed over the course of five months (Table 1). The tropical locations of Puerto Rico, the Amazon (TRMM-LBA), Maldives, Sumatra, Manus, and Darwin (green-colored bars in Fig. 3) collectively account for 27% of the relative number of large raindrop spectra sampled. The subtropical locations of Wallops, Hiratsuka, Oklahoma, Huntsville, Florida [TRMM Texas and Florida Underflight Experiment (TEFLUN-B)], and Okinawa (blue-colored bars in Fig. 3) collectively account for 30% of relative number of large raindrop spectra sampled. The locations listed in Table 1 that have climates characterized as continental and Mediterranean–semiarid are represented in Fig. 3 by the gray-colored and orange-colored bars, respectively.

The greatest number of large raindrops per large raindrop spectra sampled was at Koto Tabang, West Sumatra, Indonesia, which is nestled within the western mountains on the island of Sumatra. An average of 5–6 large raindrops was found in the 288 min of large raindrop spectra that were sampled over the course of 265 rainy days at this location. In Puerto Rico the average number of large raindrops in each large raindrop spectrum was only between 3 and 4, despite having the greatest percentage of raindrop spectra to contain large

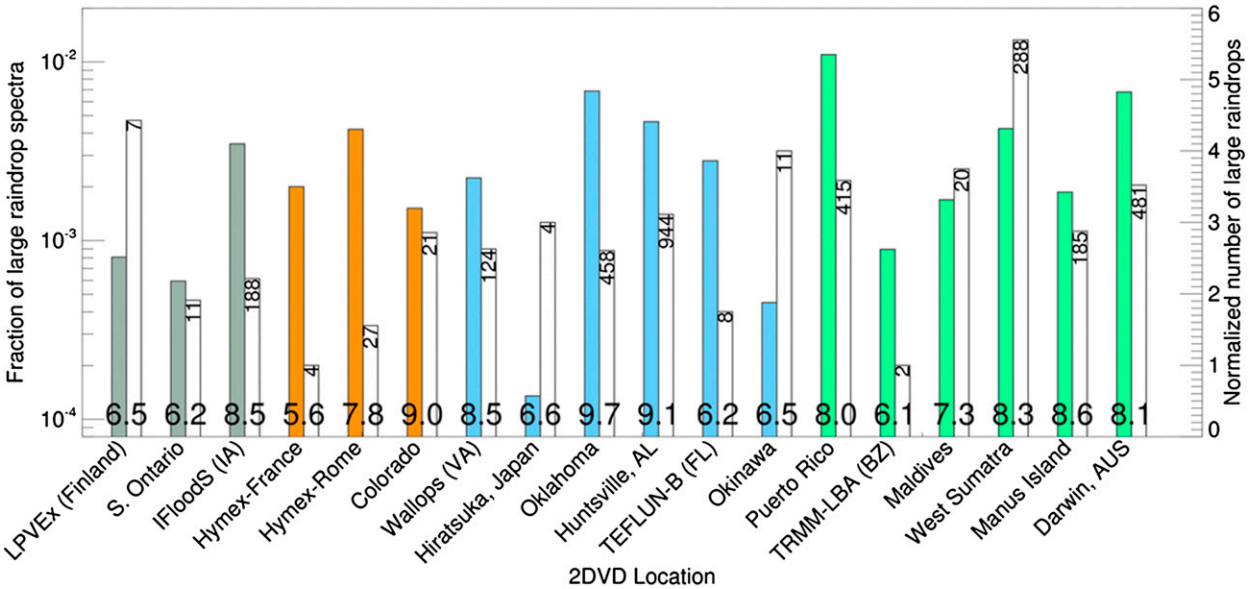

FIG. 3. An overview of large raindrops sampled by one or more 2DVD(s) at the locations in Table 1. The colored bars, which represent climatological regions and are defined in the text, are the fraction of 1-min raindrop spectra containing large raindrops; the white bars are the total number of large raindrops normalized by the total number of 1-min raindrop spectra that contained large raindrops. The number of 1-min spectra containing one or more large raindrops is labeled within the white bars, and D_{max} (mm) found at each location is labeled along the abscissa.

raindrops. In southern Finland [Light Precipitation Validation Experiment (LPVEx)], less than 0.1% of the raindrop spectra sampled during September and October of 2010 contained large raindrops, but an average of 4–5 large raindrops occurred in each large raindrop spectra sampled. However, the relatively high average number of large raindrops found in each large raindrop spectrum sampled in Finland may not be truly representative of typical large raindrop production efficiency here. Only 31 large raindrops were found to occur in southern Finland, and all were contained within only seven of the 1-min raindrop spectra, which were sampled by two of the three 2DVDs deployed during a two-month period. A median value of 3–4 large raindrops occurred in large raindrop spectra sampled in the tropical locations, whereas a median value of 2–3 occurred in those sampled in subtropical locations (Fig. 3).

The largest raindrop observed at each location is labeled above the abscissa of Fig. 3. The largest raindrop was found in Oklahoma, and further elaboration about this event will be provided toward the end of this section. Taking into account all of the 2DVD observations included in this dataset, a total of nearly 9637 h of rainfall was used to construct a monthly and hourly climatology of large raindrops.

b. *Seasonal and diurnal occurrence of large raindrops*

The monthly occurrence of large raindrops at each location is provided in Fig. 4. Only locations where rainfall was sampled each month of the year were included for this comparison. We found the most large raindrops during April and May in Oklahoma and Huntsville, respectively (Figs. 4a,b). This trend was present even after normalization to reduce the sampling bias (i.e., the greatest fraction of raindrop spectra contained large raindrops during these months). In Puerto Rico, August and September were found to have not only the greatest number of large raindrops sampled but also the greatest fraction of raindrop spectra that contained large drops (Fig. 4c). No large raindrops were found in Puerto Rico during the months of February and March, but these months combined only accounted for roughly 3% of the total number of rainy minutes sampled there.

The equatorial location of West Sumatra had the greatest number of large raindrops sampled in November and the most raindrops ($D_{eq} \geq 0.2$ mm) in January and December (Fig. 4d). We found 241 large raindrops fell during 8 days in November, whereas 132 large raindrops fell during only two days in July. Most of the large raindrops and large raindrop spectra sampled in West Sumatra occurred between September and November. Much less annual variability was found on Manus Island, where the total number of raindrops sampled was around 2–5 million each month (Fig. 4e). The fewest number of large raindrop days and 1-min raindrop spectra sampled on Manus Island occurred in May and November, but a seasonal pattern is not readily

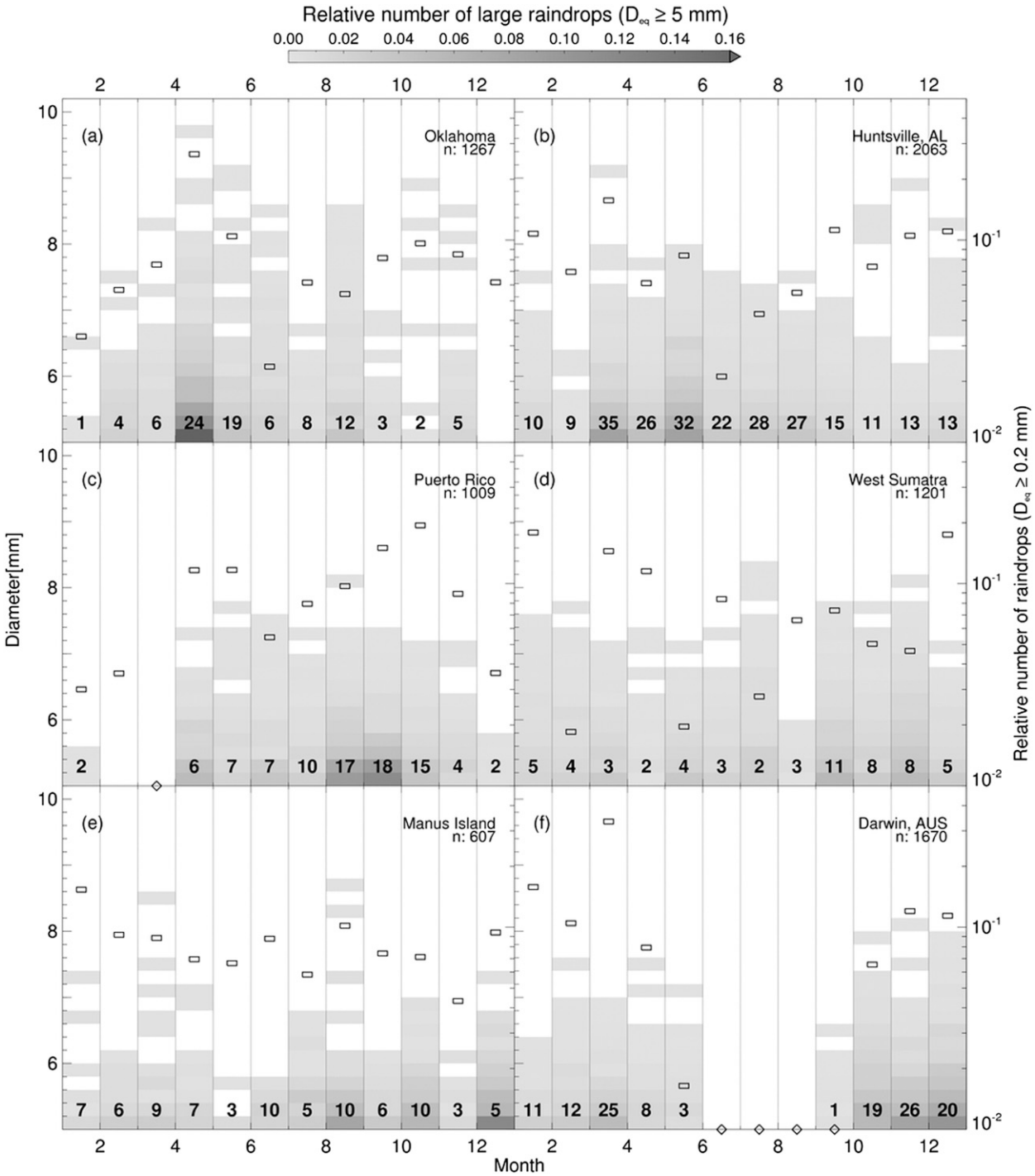

FIG. 4. Monthly number of raindrops sampled. (a)–(f) Locations where 2DVD(s) measured raindrop spectra each month of the year. The spectrum of large raindrops (relative to the total at each location) is shaded, and the relative number of monthly raindrops ($D_{eq} >$ 0.2 mm) is given by the open rectangles. Months with at least one or more raindrops that contributed <1% of the total number of raindrops sampled are indicated by diamonds along the abscissa. The total number of days on which one or more large raindrops were sampled each month is listed along the abscissa. The total number of large raindrops sampled is given in the upper right of (a)–(f).

apparent. Also, 607 large raindrops were sampled on Manus Island, which is half that sampled in West Sumatra even though nearly 2600 more raindrop spectra were sampled by the 2DVD on Manus Island (Table 1).

A very pronounced seasonal precipitation cycle was found in Darwin, Australia (Fig. 4f). Over the course of nearly three years, 1670 large raindrops were sampled here, but no large raindrops were observed between June and August. Large raindrop occurrence exhibited a peak during the transitional seasons, particularly the months of March and November. The total number of raindrops ($D_{eq} \geq 0.2$ mm) sampled in Darwin followed a similar pattern.

Most of the large raindrops sampled at each location throughout the year were less than 6 mm in diameter, but raindrops exceeding 8 mm in diameter were found at each location included in Fig. 4, especially in Oklahoma. The largest raindrops in Oklahoma and Huntsville occurred during the spring months, and the largest raindrops in the tropical locations of Puerto Rico, West Sumatra, and Manus Island occurred during July and August. The largest raindrops at nearly each of these locations occurred during months that had the most large-raindrop days sampled (Fig. 4). However, in West Sumatra, the largest raindrop occurred during the month of July, which interestingly had the fewest number of large raindrop days sampled (Fig. 4d).

The hourly occurrence of large raindrops was examined at each of the 18 locations (Fig. 5). Locations where concentrated 2DVD measurements were made during specific times of the year (e.g., field campaigns listed in Table 1) cannot be compared with other locations that had a much longer record of 2DVD measurements because of annual variability of the diurnal precipitation cycle. For example, the 2DVD measurements in Rome were only during September and October of 2012, which is typically the time of year when afternoon convection peaks in that region of the Mediterranean (Ducrocq et al. 2014). However, they were included to serve as a reference for future study.

The number of large raindrops that were sampled each hour peaked during the afternoon at 17 of the locations examined, although it was weak at some of them. No daytime peak in large raindrop occurrence was found at West Sumatra. Only five large raindrops were found to occur during the daylight hours in West Sumatra, but they all occurred within a few hours of sunrise (Fig. 5p). No large raindrops were found to occur at this location during the daytime hours after 0900 LT (i.e., 99% of the large raindrops occurred when the sun was below the horizon), even though 42% of the raindrops sampled occurred during the day.

A disproportionate number of large raindrops were also found in Oklahoma when the sun was below the horizon (Fig. 5i). Over 47% of the large raindrops sampled in Oklahoma were during the night, mostly just before sunrise. Over 12% of the large raindrops in Oklahoma occurred between 0500 and 0600 LT. The raindrops sampled by 2DVDs in Iowa during the spring of 2013 (Fig. 5c) exhibited similar diurnal trends to those in Oklahoma, which were sampled over the course of more than two years (Fig. 5i). The 2DVDs in Huntsville, which is at a latitude similar to the Oklahoma 2DVDs, sampled 63% of the large raindrops during the day, but the largest hourly occurrence was between 2000 and 2100 LT (Fig. 5j).

There was a clear diurnal trend of raindrop occurrence in Puerto Rico (Fig. 5m), where 2DVD observations were obtained at two different parts of the island collectively over the course of 18 months (Table 1). Nearly 85% of the large raindrops sampled here occurred between 1000 and 1600 LT. The raindrops sampled on Manus Island also exhibit a peak during the day and minimum at night, but the number of large raindrops sampled here increased much more gradually throughout the day (Fig. 5q). Similarly, the hourly number of large raindrops sampled at Darwin also did not exhibit any significant diurnal trend (Fig. 5r).

West Sumatra had the highest hourly concentration of large raindrops among the six locations where raindrops were sampled all 12 months of the year. Over 32% of the large raindrops occurred here between the hours of 2100 and 2200 LT. Puerto Rico had the second highest concentration at 24% between 1400 and 1500 LT, but the other four locations—Huntsville, Oklahoma, Manus, and Darwin—did not have such high hourly concentrations. Their peak hourly concentration was less than 16%.

c. *Giant raindrops*

There were 41 raindrops exceeding 8 mm in diameter in the 2DVD data we considered. Raindrops of this size, which are referred to herein as giant raindrops, occurred at both tropical and subtropical locations (Fig. 3). Although the longest period of 2DVD measurements took place in Huntsville, 22 of the giant raindrops were sampled in Oklahoma, largely during the spring months (Fig. 4a). Most of the giant raindrops occurred in the subtropical locations, but nine of the giant raindrops considered were in tropical locations, including four of them in West Sumatra, three in Manus, one in Darwin, and one in Puerto Rico. The largest raindrop sampled at these tropical locations had a D_{eq} of 8.6 mm and occurred at the U.S. Department of Energy (DOE) Atmospheric Radiation Measurement Program (ARM) site on Manus Island, Papua New Guinea, on 21 August 2013.

At least one giant raindrop was sampled at locations where more than 27 900 min of raindrop measurements

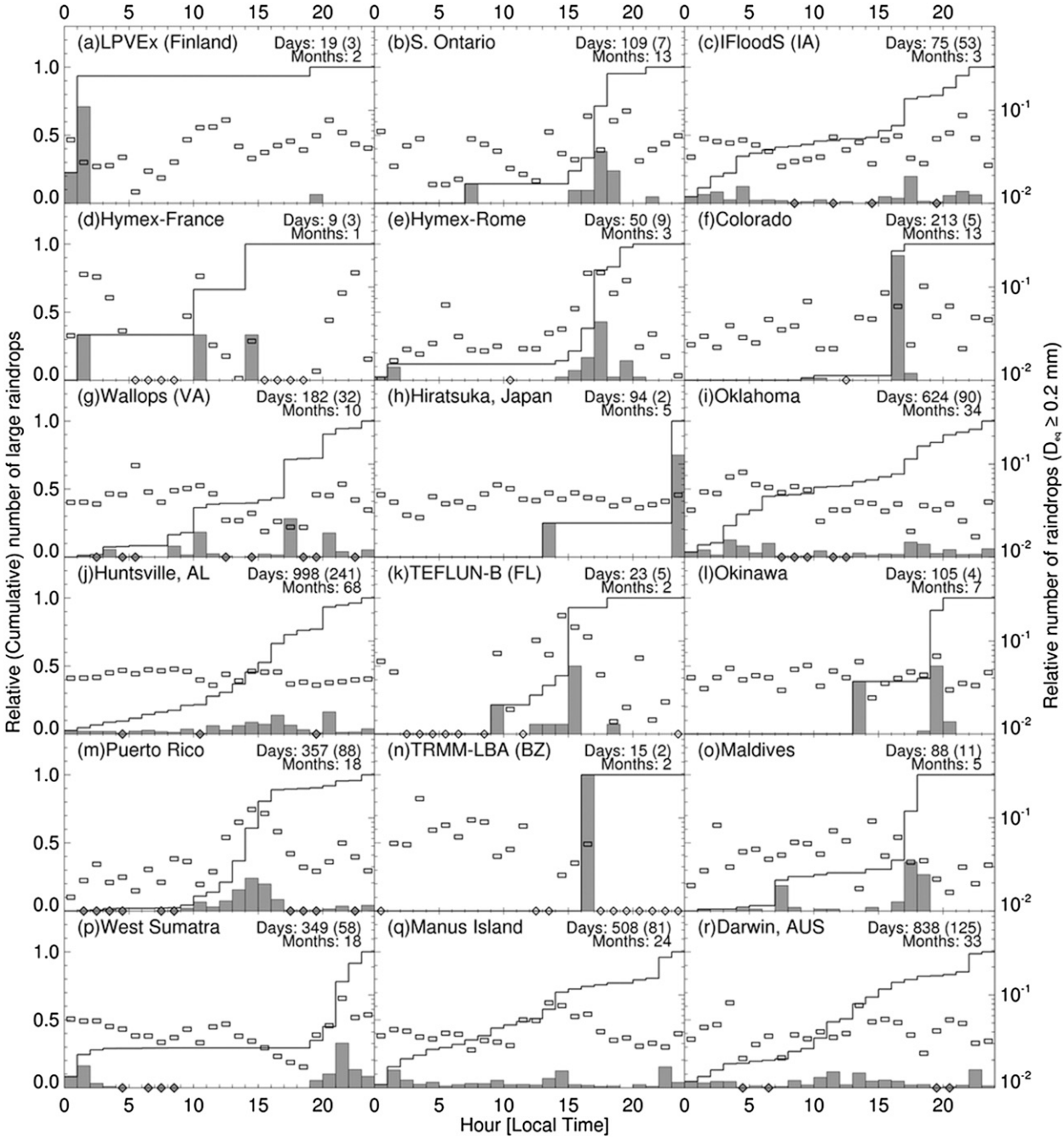

FIG. 5. Hourly number of raindrops sampled at each of the locations listed in Table 1. The hourly distribution of large raindrops (relative to the total at each location) is given by the bars, and the cumulative hourly distribution of large raindrops is the solid line. Hours with at least one or more raindrops (large raindrops) that contributed <1% to the total number of raindrops (large raindrops) sampled are indicated by the open (filled) diamonds along the abscissa. The relative number of hourly raindrops ($D_{eq} > 0.2$ mm) is given by the open rectangles. The total number of days (those with large raindrops sampled) and number of months that were sampled are given in the upper right of (a)–(r).

were made (Table 1), with the exception of Colorado where only one very giant drop was found among the 13 841 min of 2DVD measurements collected there. The shape of this 9.0-mm raindrop found in Platteville, Colorado, on 10 September 2006 matches that of a large, oblate raindrop, but it had a fall velocity slightly exceeding its "expected" terminal velocity (Gunn and Kinzer 1949; Atlas et al. 1973), even after adjustment for that location's altitude above mean sea level (Beard 1985). It is worth mentioning that the Atlas et al. (1973)

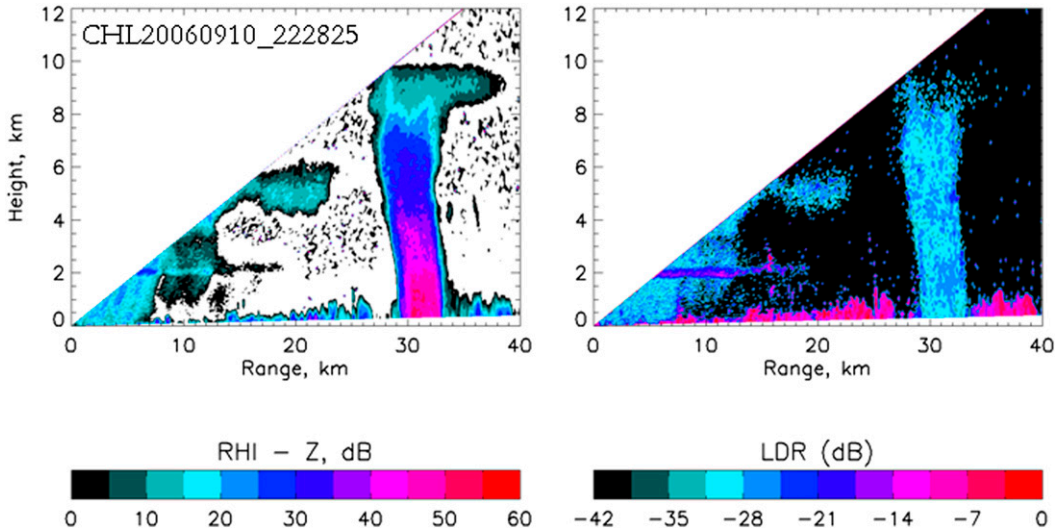

FIG. 6. CSU–CHILL radar RHI scans of (left) radar reflectivity (dBZ) and (right) linear depolarization ratio (dB) over the 2DVD site at Platteville (30.4-km range) at 2228 UTC 10 Sep 2006.

terminal velocity expression was only fitted to raindrops with diameters no larger than 5.8 mm. However, 2DVD measurements by Thurai and Bringi (2005) indicate most 6-mm or larger raindrops have fall velocities slightly below the Atlas et al. (1973) terminal velocity curve (also see Fig. A1a). So it is interesting that the fall velocity of this 9.0-mm raindrop exceeds that expected. This event was captured, to a large extent, by the CSU–CHILL S-band polarimetric radar (Brunkow et al. 2000) located approximately 30 km from the Platteville 2DVD site. Figure 6 shows this giant raindrop in Colorado was produced by an isolated and intense rain cell with a 50-dBZ reflectivity core and echo top near an altitude of 10 km. Linear depolarization (LDR) measurements indicated no presence of hail aloft (Fig. 6). Very narrow sector scans at constant elevation angle revealed that differential reflectivity Z_{dr} reached its greatest value near 4 dB just after 2230 UTC, when the 2DVD recorded a D_{max} of 9.0 mm.

The biggest raindrop found in this dataset had a D_{eq} of 9.7 mm and was observed in northern Oklahoma at the ARM Central Facility site operated by the DOE. A reconstructed three-dimensional image of this very giant raindrop, which was recorded by the DOE's compact-version 2DVD, is shown in Fig. 7. Its shape is very similar to the raindrop shape contours computed by Thurai et al. (2007), which was determined from more than 115 000 drops. This raindrop was produced by a left-moving supercell storm, which is commonly known to be a large hail-bearing type of storm (Bunkers 2002), that occurred during the overnight hours of 29 April 2012. The 2DVD also recorded some partially melted hail, similar in shape to that described by Rasmussen et al. (1984), as this storm passed over the site. Thus the existence of a small ice core within the 9.7-mm hydrometeor cannot be ruled out, but is very unlikely given its shape (Fig. 7). Furthermore, 1 min prior to when the 9.7-mm raindrop was recorded, dual-polarimetric measurements from the NEXRAD at Vance, Oklahoma, which is located about 55 km away, indicated that the precipitation over the ARM Central Facility was dominated by high Z_{dr} around 3–4 dB, specific differential phase K_{DP} of 3 dB km^{-1} and a hail detection ratio (HDR; Aydin et al. 1986) $\ll$ 0 dB, similar to the CSU–CHILL radar measurements of the 9.0-mm raindrop in Platteville. Another raindrop exceeding 9 mm in diameter was found in this dataset, and it was recorded by CSU's low-profile 2DVD in Huntsville on 5 March 2013 at 1756 UTC. This raindrop had a D_{eq} of 9.1 mm, and as its parent storm moved across the Huntsville area, several instances of 2.5-cm hail at the ground were reported.

d. D_{max}–D_m characteristics

Although this study was geared toward the tail of the DSD, observations of the entire DSD in the size ranges considered (i.e., $0.2 \leq D_{eq} < 12.0$ mm) were used to examine the relationship between D_{max} and D_m. The 240 million raindrops were integrated to yield 346 713 one-min DSD spectra, which, to obtain a robust sample size, were each required to contain at least 100 raindrops. The D_m was computed from these measured spectra as the ratio of the fourth and third moments of the DSD. The resultant distribution of D_{max}/D_m was positively skewed with a median D_{max}/D_m ratio of 1.8,

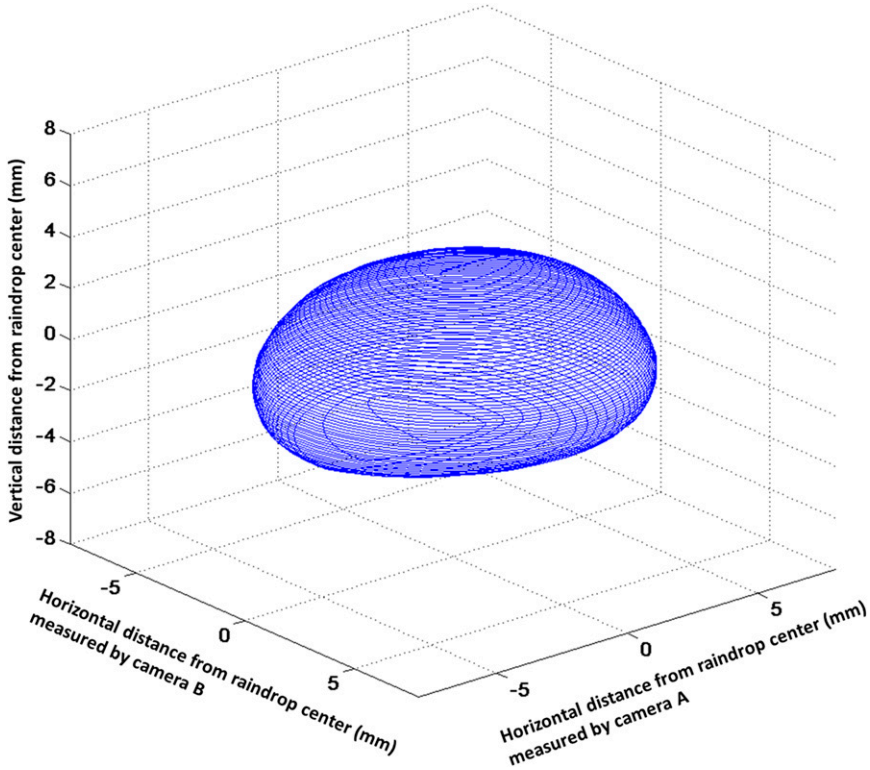

FIG. 7. A 3D reconstruction of the 9.7-mm raindrop that was recorded by the DOE's 2DVD at their ARM Central Facility site in Oklahoma at 0540 UTC 29 Apr 2012.

and 90% of the spectra had a ratio between 1.4 and 2.7 (Fig. 8). This ratio was found to increase from 1.5 at a rainfall rate of 0. 1 mm h^{-1} to 2.2 for rainfall rates exceeding 50 mm h^{-1}.

We also examined the behavior of $D_{\max}/D_m$ as function of the reflectivity factor (i.e., sixth moment of the DSD) for these 1-min DSDs (Fig. 8). The distribution of reflectivity factor Z was nearly a perfect Gaussian (in dBZ units) with a geometric mean of 20.8 dBZ and standard deviation of 9.3 dB. The $D_{\max}/D_m$ ratio of 1.5 was roughly constant for $-5 < Z < 10$ dBZ and increased 33% for $10 \leq Z < 25$ dBZ, whereas the ratio remained around 2.0 with less than 12% variation for larger values of Z.

4. Discussion

a. Large raindrop occurrence and their source

The peak in large raindrop occurrence during the springtime in Huntsville and Oklahoma as well as during the premonsoon season in Sumatra, Manus, and Darwin (Fig. 4) suggest that the deep convective storms, which often occur during this transition season, are favorable for large raindrop formation. The strong vertical motions present in such clouds enhance the collision efficiency and thus increases the chance for large raindrops to develop, especially in those clouds containing an abundance of liquid water. Deep convective clouds can also have all the necessary ingredients required for hail formation.

The trend in the monthly occurrence of large raindrops (Fig. 4) is similar to that of the global severe hail climatology constructed from satellite passive-microwave observations by Cecil and Blankenship (2012). They found an annual maximum of large-hail-producing storms occurs in late spring, which agrees well with the large raindrop peak we found in the subtropical locations (Figs. 4a,b) as well as the tropical locations (Figs. 4c–f). In fact, many of the 1-min integrated 2DVD measurements consisting of giant raindrops were also found to contain partially melted hail. This suggests many of the large, and especially giant, raindrops in the 2DVD dataset presented herein may have previously been hail, similar to what others have inferred from dual-polarimetric radar measurements (e.g., Ryzhkov and Zrnić 1995, 1996; May et al. 2001; Schuur et al. 2001). It does not mean that hail must reach the ground, nor does it mean that hail aloft is the source of all large raindrops. Large raindrops have also been found in warm-rain clouds (e.g., Beard et al. 1986; Rauber et al.

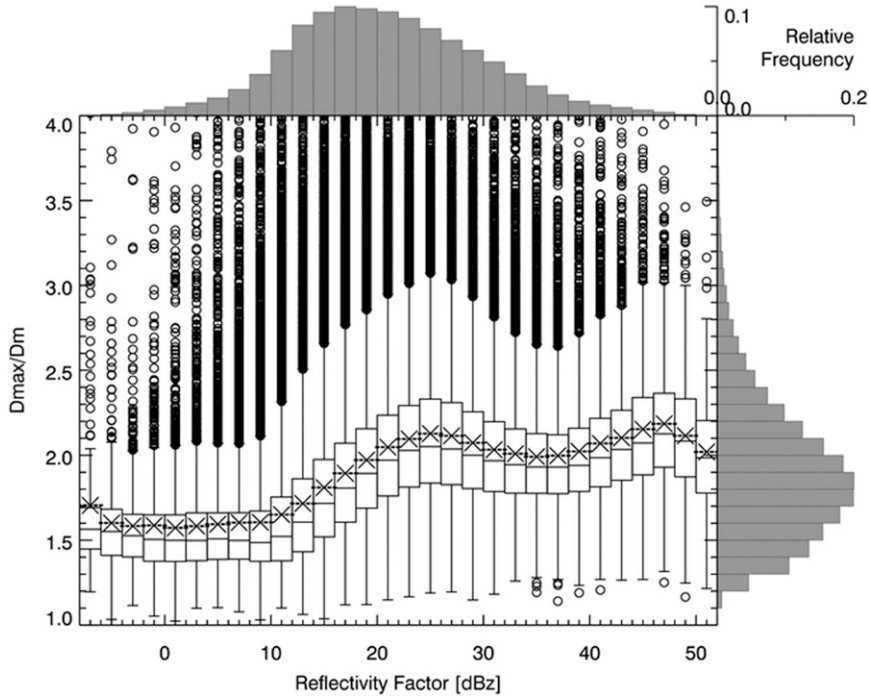

FIG. 8. Box-and-whisker plots for the ratio of maximum raindrop diameter (D_{max}) and mass-weighted mean diameter (D_m) as a function of Z in each 1-min raindrop spectrum containing at least 100 drops. Tops and bottoms of boxes represent the 75th and 25th quartiles, respectively. The horizontal solid lines inside the boxes represent the median, and the dashed lines with a times sign represent the mean ratio in each bin. Tops and bottom of the whiskers represent 150% of the interquartile range (IQR). The circles represent outliers (i.e., 1-min DSDs with a D_{max}/D_m ratio exceeding 150% of the IQR). The relative distribution of Z is given atop the plot, and the relative distribution of D_{max}/D_m is given on the right of the plot.

1991; Takahashi et al. 1995; Baumgardner and Colpitt 1995; Hobbs and Rangno 2004). Actually, a far greater number of large raindrops examined in this 2DVD dataset were found in the tropics, where hail rarely reaches the ground (Frisby and Sansom 1967; Barnes 2001). Although this suggests collision and coalescence between raindrops may also be a source of large raindrop formation (e.g., Rauber et al. 1991; Szumowski et al. 1998), it does not imply that large raindrops are more likely a result of warm-rain processes than melted hail. The melting layer in tropical locations is typically at such a high altitude that hail melts before reaching the ground. According to the melting model of Rasmussen and Heymsfield (1987), hailstones with initial diameters between 8 and 15 mm that fall from a height of 4 km can completely melt, especially in a humid environment like the tropics, to form 8-mm raindrops (Ryzhkov et al. 2013). UHF profiler observations (Kobayashi and Adachi 2001) indicate large raindrops may appear and disappear from the DSD spectra as they evolve toward the ground. Initially large raindrops may be the result of a melted hailstone, but quickly breakup into smaller raindrops that in turn may collide and coalesce to again form a large raindrop.

Less than 0.5% of the 1-min raindrop spectra sampled by the 2DVDs contained large raindrops. The greatest fraction of raindrop spectra containing raindrops 5 mm or larger was found at tropical locations (Fig. 3). The greatest concentration of large raindrops were found during the transitional period just prior to the monsoon season in Sumatra, Manus, and Darwin (Fig. 4), and all but Darwin had large raindrops sampled each month of the year. Although less than 10% of the rain that falls in Darwin occurs between May and September (Nicholls et al. 1982), some parts of northern Australia received considerably below average rainfall in 2012 and 2013 (Beard et al. 2013; Chappell et al. 2014)—two of the three years for which 2DVD measurements were available at Darwin (Table 1).

Puerto Rico had the greatest fraction of 1-min raindrop spectra containing at least one large raindrop, which indicates large raindrops are most likely to be found at these two locations in Puerto Rico (San Juan and Mayagüez) than any of the other locations examined

in this study. This may be explained by two reasons. First, much of Puerto Rico consists of mountains, which enhance vertical motion and thus rain production, especially during the afternoon when the sea-breeze circulation is active. Second, barotropic environments are composed of weak vertical wind shear, which allow individual precipitating clouds to sit over the same location and thereby increase the chance that a large raindrop would be sampled by a 2DVD. Although Puerto Rico is affected by tropical cyclones, these synoptic-scale phenomena are largely characterized by raindrops less than 5.0 mm in diameter (Tokay et al. 2008).

The greatest average number of large raindrops sampled per rainy minute was found in Koto Tabang, West Sumatra. This region receives some of the greatest amounts of rainfall on Earth (Adler et al. 2003; Mori et al. 2004). The 2DVD here was located in the sharply rising mountains at an altitude of 865 m MSL on the western side of the island where similar atmospheric–land interactions are also at work. However, raindrop occurrence in Puerto Rico roughly follows the diurnal solar cycle, whereas we found the opposite in West Sumatra (Figs. 5m,p). The 2DVD measurements in Puerto Rico were along the coast where the sea-breeze front produces convection in the early afternoon before it moves farther inland. A much smaller, but secondary peak of large raindrops were found in Puerto Rico in the late evening as the sea-breeze front retreats (Fig. 5m). The 2DVD location in West Sumatra was slightly farther inland and on the eastern slopes of a mountain range with an orientation and location relative to the coastline that can lead to somewhat more complex land–ocean breeze circulations, which locally enhance precipitation during the late evening (Mori et al. 2004; Biasutti et al. 2012).

It is interesting that no large raindrops were found to occur at Koto Tabang during the daylight hours even though 42% of the raindrops sampled here occurred during the daytime. Perhaps this is due to the nature of daytime versus nighttime convection that occurs in this region of Indonesia. The global lightning climatology composed by Virts et al. (2013) using satellite and ground-based sensors reveals little lightning activity over the western half of Sumatra during the daytime. However, lightning activity becomes greatest over this region during the early evening hours—around 1800–2000 LT. Biasutti et al. (2012) found the concentration of precipitation moves downslope during the late afternoon and is focused along the western and eastern slopes during the evening, which is when the most large raindrops were sampled by the 2DVD at Koto Tabang (Fig. 5p). Thus the deeper convective clouds that contain ice are likely responsible for the large raindrops observed at night, and may be complemented by stratiform remnants of earlier convection (Mori et al. 2004). Shallower, warm-rain clouds that occur during the day in West Sumatra are not as conducive to producing large raindrops. However, shallow, warm-rain clouds have been found to contain large raindrops, albeit at or near cloud base (e.g., Beard et al. 1986; Takahashi et al. 1995; Hobbs and Rangno 2004). Thus the lack of large raindrops in the 2DVD measurements at Koto Tabang that are likely produced by similar precipitating clouds during the day over Sumatra warrants further investigation. We speculate that large and especially giant raindrops found near the base of warm-rain clouds rarely reach the surface intact, or are not as likely as that resultant from melted hail because the ice core of melting hail makes the raindrop more stable than without it (Rasmussen et al. 1984).

The greatest fraction of large raindrops found in Oklahoma and Iowa occurred overnight, but during the latter half of the daytime in Huntsville (Figs. 5c,i,j). Mesoscale convective systems (MCSs; Maddox 1980), which often initiate after sunset during the warm season in the Great Plains and can account for as much as 70% of the seasonal rainfall (Fritsch et al. 1986), are the likely reason for the disproportionate number of large raindrops found at night in Oklahoma and Iowa compared to Huntsville. The broad area of trailing stratiform precipitation characteristic of MCSs is composed largely of hydrometeors that develop from the ice phase and can contain large aggregates (Stewart et al. 1984; Willis and Heymsfield 1989; Smith et al. 2009). Thus melted aggregate snowflakes could also be a source of large raindrops.

It is worth mentioning that many of the 2DVD measurements during times of cold weather (i.e., hourly temperatures below 3°C), which included many cold-rain events, were blindly removed from this dataset, and thus the large raindrop numbers reported herein are likely underestimated. The standard processing performed by the 2DVD software assumes all objects in its measurement area behave as oblate spheroids with a vertical axis of symmetry (Schönhuber et al. 2008), which can cause snowflakes to have incorrect characteristics. We visually inspected a few raw camera "images" during one cold-rain event and found snowflakes had made it through our filtering method (section 2c) as a result. Thus cold-rain events were removed to avoid melting or mixed-phase particles from being included in the raindrop dataset. However, these cold-rain events may have produced some of the largest raindrops. Using a 2DVD, Fujiyoshi et al. (2008) found a 9.2-mm raindrop in winter stratiform precipitation (Table 2).

TABLE 2. Survey of other large raindrop observations during natural rainfall.

Study	D_{eq} (mm)	Location	Date	Instrument
Fujiyoshi et al. (2008)	9.2	Kanazawa, Japan (at the ground)	0840 UTC 16 Dec 2004	2DVD
Takahashi et al. (1995)	9	Manus Island, Papua New Guinea (above cloud base)	December 1991 and November 1992	Videosonde (balloonborne)
Fujiyoshi et al. (2008)	8.6	Sumatra, Indonesia (at the ground)	2004; 2005	2DVD
Hobbs and Rangno (2004)	8.2	Northern Brazil; Kwajalein Atoll, Marshall Islands (cloud base)	September 1995; July 1999	PMS 2D-P (aircraft-mounted probe)
Beard et al. (1986)	8.2	Hawaii (below cloud base)	23 Jul 1995	PMS 2D-P (aircraft-mounted probe)
Zrnić et al. (2000)	8	Tiwi Islands, Australia (2.5 km AGL)	November–December 1995 [Maritime Continent Thunderstorm Experiment (MCTEX)]	Videosonde (balloonborne)
Chang (2012)	7.5	Southern Taiwan (at the ground)	0634 UTC 31 May 2008	2DVD

Only 0.4% of the *large* raindrops we found exceeded 8 mm in diameter. Giant raindrops must overcome a great amount of hydrodynamic instability to resist breakup—a raindrop exceeding 9 mm in equivalent spherical diameter is very unlikely to reach the ground, especially given that only four were found among the 240 million raindrops examined in this study. However, raindrops exceeding 9 mm in diameter have also been found in natural rainfall near cloud base by Takahashi et al. (1995) and at the ground by Fujiyoshi et al. (2008). In addition to those found to occur in nature, Thurai and Bringi (2005) measured a water drop of 9.5 mm in their 80-m bridge experiment, albeit using a water hose to simulate the rainfall, and Pruppacher and Beard (1970) measured a simulated raindrop with a diameter around 9.2 mm in their wind tunnel experiment. Thus raindrops exceeding 9 mm in diameter are possible. The 9.7-mm raindrop we found in the 2DVD dataset collected in Oklahoma is larger than any of those listed in Table 2 as well as those found in simulated rainfall (e.g., Pruppacher and Beard 1970; Thurai and Bringi 2005; Szakáll et al. 2010). So exactly what conditions must be present to allow such a giant raindrop to develop? Although a definitive answer to this question is beyond the scope of this study, the observations and brief radar analysis presented herein support the hypothesis that raindrops this large most likely result from hail that has completely melted just prior to reaching the ground. However, CSU–CHILL measurements of the deep convective cloud that produced the 9.0-mm raindrop in Platteville had LDR values that were very low (<-28 dB), indicating that there was likely no hail aloft, although graupel may have been present. Upon melting, the graupel would have a large sweep out area for collision with smaller raindrops. Thus this particular very giant raindrop may have formed initially as a result of melted graupel and grew via the warm-rain process. However, it is interesting that the fall velocity of this 9.0-mm raindrop exceeded that expected, which seems to suggest the raindrop either contained (or very recently contained) an ice core or perhaps was accelerated by downdraft air.

b. D_{max} *implications*

In our dataset of more than 346 713 min of raindrop spectra, we found a maximum diameter of 9.7 mm and a spectrum that contained a D_{max} 15 times as large as D_m. However, the median value of D_{max} was 1.8 times that of D_m, which is only slightly greater than that computed by Smith et al. (1993) from statistical sampling simulations. Smith et al. used a sample size of 500 raindrops to arrive at a median value of $D_{max} = 1.7D_m$, whereas we considered only spectra containing 100 raindrops but for 1-min DSDs measured at 18 diverse geographical locations (Fig. 2). However, our D_{max}/D_m distribution was highly positively skewed and thus a ratio of 1.8 is likely an underestimate of the true population value. This supports the findings of Smith et al. (1993)—it is simply not possible to practically determine D_{max} using 2DVDs (i.e., point measurements).

Large and especially giant raindrops can have a great impact on radar variables like Z_{dr}. The 1-min DSD that included the 9.0-mm raindrop measured by the 2DVD in Colorado was used to simulate radar measurements of

Z_{dr} at several radar frequencies via the T-matrix method (Bringi and Chandrasekar 2001, appendix 3). The simulated Z_{dr} was 4 dB at S band, which agrees with the peak Z_{dr} values measured by the CSU–CHILL radar around the time the 2DVD recorded the 9.0-mm raindrop. In rain regions without large drops, the CSU–CHILL measured Z_{dr} around 0.5–1.5 dB, which is a more typical value measured in rain. The 9.0-mm DSD yielded a simulated Z_{dr} of 6.5 dB at C band (because of non-Rayleigh scattering effects) whereas at X and Ku band, the simulated Z_{dr} was 4 and 3.4 dB, respectively. This clearly shows the importance of D_{max} in radar simulations, particularly for Z_{dr} at C band, which has also been shown by Keenan et al. (2001) and Carey and Petersen (2015).

It was especially surprising to find D_{max}/D_m exhibited a marked increase for $10 < Z < 25$ dBZ but was relatively constant for $Z > 25$ dBZ. Thus D_m must begin to increase relative to D_{max} around 25 dBZ. After further investigation we found both D_{max} and D_m increased with Z, but the rate of D_{max} change with respect to Z increased by a factor of 3 between 15 and 25 dBZ, whereas the rate of D_m change with respect to Z exhibited little change for $Z < 25$ dBZ. Around 25–30 dBZ, the rate of D_m change with respect to Z increased by a factor of 2, whereas D_{max} also increased but at a lower rate across this range of Z. These changes in rate (or slope) of D_{max} and D_m with respect to Z are the mathematical reason for the observed D_{max}/D_m trend in Fig. 8, but it is unclear whether this change in behavior of both D_{max} and D_m was due to a physically occurring process that we have sampled or simply due to our disproportionate sample sizes, which were obtained from different climatological regimes, some with periods of concentrated sampling (Table 1). If proven to be a valid feature, the jump in the D_{max}/D_m ratio around 10 dBZ could be exploited by radar retrieval algorithms to obtain a more robust estimate of D_{max}.

5. Summary

Raindrop observations from 2DVDs deployed at 18 diverse geographical locations have been compiled in this study to help validate common D_{max} assumptions used in the retrieval of rainfall rate and water content from both active and passive remote sensing measurements, like those obtained with the GPM *Core Observatory* satellite (Hou et al. 2014). A total of 775 664 one-min raindrop spectra containing more than 240 million raindrops sampled by 2DVDs were searched for raindrops exceeding 5 mm in equivalent spherical diameter (i.e., large raindrops). Large raindrops were found in less than 0.5% of these 1-min spectra, and 44% of the large raindrop spectra occurred in the tropical locations where only 31% of the raindrops ($D_{eq} \geq 0.2$ mm) in our 2DVD database were sampled. Large raindrops occurred at each location, but were most frequent and abundant at tropical locations, especially on the islands of Puerto Rico and Sumatra. This finding may be exploited to adjust DSD assumptions used for retrieval of rainfall characteristics in the tropics (e.g., use a broader DSD shape in the tropics). However, there is some question as to whether large raindrops are actually more common in the tropics because of microphysical processes or if large raindrop sampling is simply more favored in a barotropic (i.e., low vertical wind shear) environment, especially on mountainous islands where there is enhanced precipitation due to atmosphere–land interactions. Evaluation of 4–6-km vertical shear above 2DVD locations could help determine if storm motion is a cause for the greater sampling of large raindrops in the tropics.

Raindrops exceeding 8 mm in diameter (i.e., giant raindrops) occurred at all locations where more than 600 h of DSDs were sampled. This finding supports the conclusions of Smith et al. (1993) that a very large number of rainfall samples are necessary to sample the largest raindrops. Since intense rainfall can be highly variable in nature, there may not be any minimum number of samples that can be predetermined, but perhaps the 600 h found in this study may provide a starting point for others trying to find naturally occurring large raindrops at similar spatial resolutions. Only 41 raindrops exceeding 8 mm in diameter were found, and 9 of these giant raindrops were found at tropical locations. Only four raindrops exceeding 9 mm in diameter were found in the entire dataset: they occurred in Colorado, Oklahoma, and Huntsville. The largest raindrop verified (i.e., shape was examined in detail) in this dataset had a D_{eq} of 9.7 mm and occurred beneath a hail-producing cloud that moved across northern Oklahoma on 29 April 2012. This giant raindrop found in Oklahoma is the largest reported in the literature to date. Although it seems impressive that a raindrop this large did not break up, 2DVD and radar measurements suggest these 9-mm and larger raindrops were recorded not long after their parent hailstone had completely melted.

The findings presented in this study suggest that large, and especially giant, raindrops that reach the ground may be the result of large melted ice such as hail. Although this is not a new idea—it has also been suggested by several others (e.g., Ryzhkov and Zrnić 1995; Zrnić et al. 2000; May et al. 2001; Schuur et al. 2001)—the dataset presented herein is the largest and most geographically diverse that has been discussed in the literature to date that supports the melted-ice hypothesis.

This large raindrop-melted hail hypothesis is corroborated by satellite passive-microwave and ground-based lightning measurements (Cecil and Blankenship 2012; Virts et al. 2013) as well as modeling studies of melting hail (e.g., Rasmussen and Heymsfield 1987; Ryzhkov et al. 2013). However, a cloud capable of generating hail may very likely have all the necessary ingredients to support large raindrop formation via warm-rain processes as well (e.g., Beard et al. 1986; Illingworth et al. 1987; Rauber et al. 1991; Bringi et al. 1991), but it is beyond the scope of this paper to examine the individual large raindrop events in further microphysical detail. Also, since melting snow aggregates may serve as another source of large raindrops (e.g., Fujiyoshi et al. 2008), a more detailed analysis of the cold-rain events excluded from this dataset should be performed to characterize the tail of the DSD for cold-rain processes.

Measurements of vertical DSD evolution are required to determine which large drop mechanism occurs most frequently. Fortunately, the 2DVD dataset compiled for this study enables large raindrop events to be readily extracted for further examination, and most, if not all, of these 2DVD deployments were collocated with, or nearby, weather radars. The cloud that produced the 9.7-mm raindrop found in Oklahoma is currently being further investigated with the wealth of radar datasets available around the DOE ARM Central Facility in Oklahoma (Thurai et al. 2014). The rainfall event that produced a 9.0-mm raindrop in Colorado is also under further examination (Thurai et al. 2014) since the CSU–CHILL radar measurements suggest that it contained no hail, whereas 2DVD measurements suggest it may have contained an ice core immediately prior to being sampled.

The 2DVD observations examined in this study yielded a median $D_{\max}$-to-D_m ratio of 1.8, which increased with rainfall rate. Thus some $D_{\max}$ assumptions commonly used in the radar community may generally be an overestimate, especially for rainfall rates below $50\,\mathrm{mm\,h^{-1}}$. Although both $D_{\max}$ and D_m were found to increase with Z, we found $D_{\max}/D_m$ to only increase over a 20-dB range of Z and was constant for $10 > Z > 25\,\mathrm{dB}Z$ (Fig. 8). We are unsure if this trend was due to a physical process we have sampled or if it was simply a result of our disproportionate sampling of different climate regimes. If it is found to be physical in nature, then this could have implications for $D_{\max}$ retrieval from radar. Thus additional study is required to further explore these possibilities.

Since this dataset consists of a large amount of raindrop size and velocity measurements from around the globe and span a range of rainfall rates, it will allow us to further examine microphysical properties and perhaps answer some of the remaining questions set forth by McFarquhar (2010), such as determining the reality of multipeaked DSD spectrum. In this study we only considered $D_{\max}$, which provides some observational guidance for selection of DSD truncation limits, but future study should further exploit either this dataset or similar ones to characterize the shape of the DSD tail, which is needed to develop suitable distribution models for DSDs containing large raindrops. This dataset also enables further testing of relationships found among DSD parameters (e.g., Williams et al. 2014) over a wide range of meteorological regimes, which is vital to retrieving accurate rainfall estimates from NASA's GPM *Core Observatory* satellite (Hou et al. 2014).

Acknowledgments. This work was supported in part by the NASA Marshall Space Flight Center Earth Science Office and the NASA Pathways Intern Employment Program. The NASA GPM GV 2DVDs were funded by Dr. Mathew Schwaller and the late Dr. Arthur Hou of NASA's GPM Project Office. The DOE 2DVD datasets were provided by the Atmospheric Radiation Measurement Program, which is sponsored by the U.S. Department of Energy, Office of Science, Office of Biological and Environmental Research, Climate and Environmental Sciences Division. The University of Iowa 2DVD dataset collected during TEFLUN-B and TRMM-LBA was kindly provided by Dr. Witek Krajewski, and the Shimane University (Japan) 2DVD dataset collected in Sumatra was kindly provided by Drs. Toshiaki Kozu and Toyoshi Shimomai. We also thank Pat Kennedy for collecting and providing the CSU–CHILL radar data presented herein. We thank the three anonymous reviewers who provided very helpful suggestions that strengthened this paper as well as Dr. Paul Smith for the insightful discussions on disdrometer sampling of $D_{\max}$. The authors are very grateful for the exceptionally gracious, continued customer support of these 2DVDs provided throughout the years by Dr. Michael Schönhuber and Mr. Günter Lammer of Joanneum Research in Graz, Austria. We are also grateful to the countless others who contributed to the deployment and careful maintenance/calibration of these 2DVDs.

APPENDIX

Filtering of 2DVD Objects by Velocity and Axis Ratio

Figure A1 provides a summary of more than 347 million, unfiltered 2DVD measurements considered in this study. Several features are readily discernable in this unfiltered dataset. There appears to be three fall velocity modes in Fig. A1a: one similar to the Gunn and Kinzer

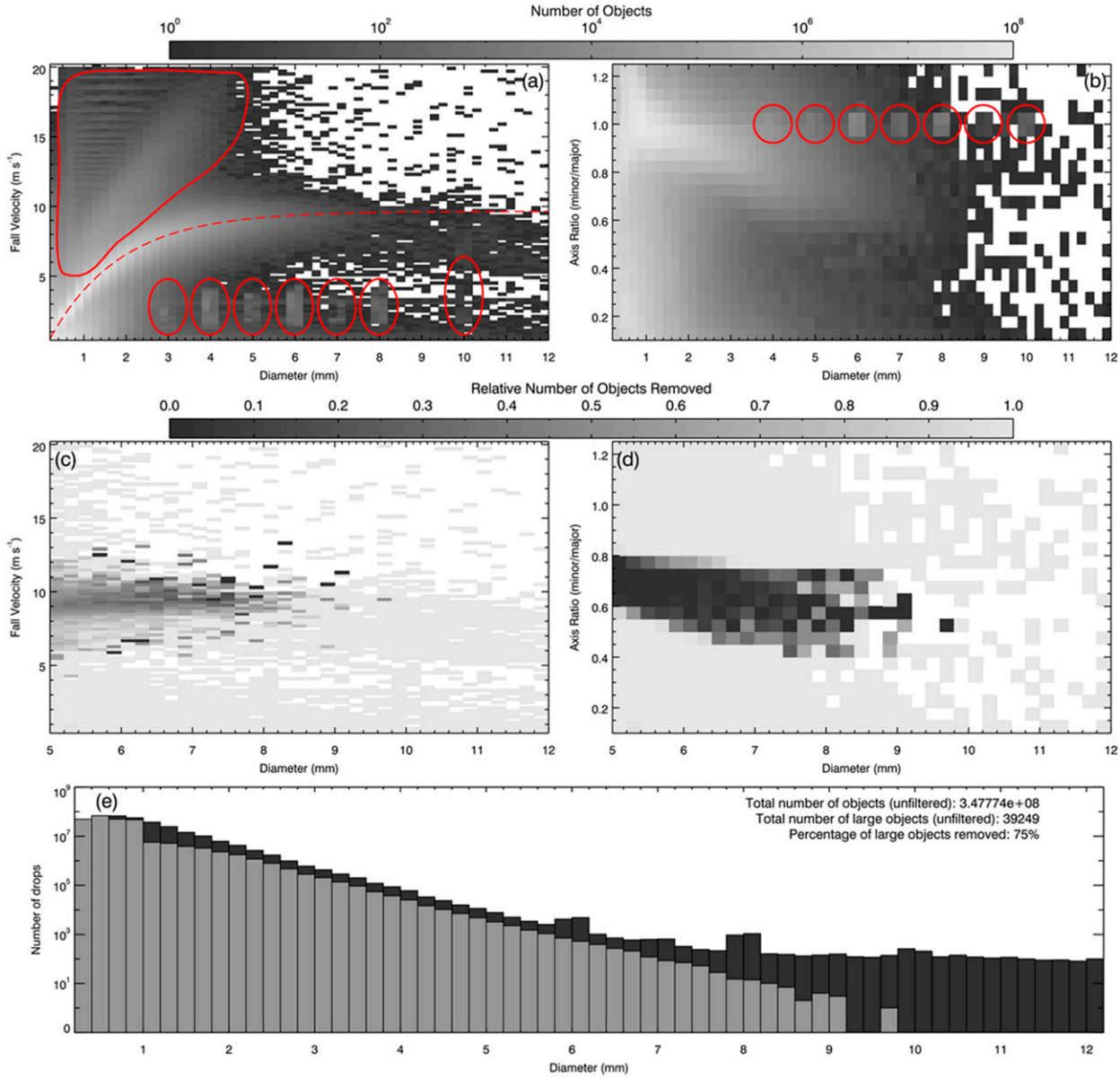

FIG. A1. Results of the filtering process applied to the 2DVD measurements compiled in this study. (a) The fall velocity and (b) axis ratio (calculated by 2DVD software) for each raindrop sampled at all locations in Table 1. The dashed line in (a) is the Atlas et al. (1973) fit to the Gunn and Kinzer dataset. The regions that are enclosed in red lines in (a) and (b) are outliers and are further discussed in the text. (c) The fall velocity and (d) axis ratio of the relative number of large raindrops removed after filtering. (e) Size distribution of all objects before (darker shading) and after (lighter shading) filtering.

(1949) terminal fall velocity measurements (dashed line); another mode likely due to objects crossing the camera field of view outside the virtual measurement area, which makes it impossible to match these objects (Kruger and Krajewski 2002; circled region above the dashed line); and a third mode of fall velocities around $3\,\mathrm{m\,s^{-1}}$, which is associated with clusters of calibration spheres centered around 3, 4, 5, 6, 7, 8, and 10 mm in diameter. These calibration spheres also readily stand out in the axis ratio plot of Fig. A1b since they are similarly clustered about their corresponding diameter and all have an axis ratio near 1. The large number of objects less than 2 mm in diameter that exists across a large range of axis ratios is possibly due to the difficulty in calculating the oblateness when a raindrop is moving with a horizontal component as well as canting about its mean vertical axis. A detailed explanation of the technique used by the 2DVD real-time processing software

to correct for such kinematic effects was provided by Kruger and Krajewski (2002) and Schönhuber et al. (2008). However, this does not appear to be much of a concern for objects exceeding 5 mm in diameter (Fig. A1c). Instead the axis ratio for most of the objects exceeding 2 mm in diameter linearly decreases with increasing diameter, which is the expected trend for raindrops (Pruppacher and Beard 1970; Beard and Chuang 1987; Thurai et al. 2009).

The terminal fall velocity of raindrops measured with the 2DVD is expected to follow that prescribed by Gunn and Kinzer (1949), which enables us to limit the dataset to only those objects that have measured fall velocities similar to that of raindrops, even for drops as large as 5–6 mm in diameter (Thurai and Bringi 2005). For larger raindrops, the Atlas et al. (1973) fit to the terminal velocities measured by Gunn and Kinzer appears to reach an asymptotic value near 9.5–10 m s^{-1} (refer to the dashed line in Fig. A1a). However, the Gunn and Kinzer dataset does not include drops exceeding 5.8 mm in diameter, and they obtained their fall velocity measurements in stagnant air. Thus some uncertainty in the fall velocity of raindrops measured with the 2DVD must be allowed, especially those exceeding 5.8 mm in diameter and for those that do not fall at their terminal velocity (e.g., because of recent collisions or contained an ice core just prior to falling through the 2DVD). Similar to other 2DVD studies, 5.8-mm or smaller drops with a fall velocity measured by the 2DVD that exceed 40% of the Atlas et al. (1973) curve were removed (e.g., Kruger and Krajewski 2002; Thurai and Bringi 2005; Tokay et al. 2013). Since the Atlas et al. (1973) curve was not fitted to larger diameter raindrops, some manipulation of this velocity threshold was required for those exceeding 5.8 mm. Several studies show the terminal velocity of drops larger than about 5–6 mm in diameter tends to decrease with increasing size (e.g., Laws 1941; Beard 1976; Thurai and Bringi 2005). This is confirmed by the downward trend in the 2DVD measurements of fall velocity for objects exceeding about 7–8 mm in diameter (e.g., Thurai and Bringi 2005; also see Fig. A1a). Thus the fall velocity filter was linearly increased from 40% at D_{eq} = 5.8 mm to 60% at D_{eq} = 10 mm (Fig. A1c). Any other large object falling outside these bounds were removed. The velocity filter accounted for 35% of the large raindrops that were removed (Fig. A1c). The axis ratio filter was applied after the velocity filtering had been performed.

The axis ratio is defined herein as the ratio of the minor to major axes of the hydrometeor. Thurai and Bringi (2005) found the mean axis ratio of raindrops measured with the 2DVD closely follows that given by the Beard and Chuang (1987) model. However, raindrop oscillations cause deviations from this model. Thus axis ratios (calculated by the 2DVD software) of objects less than 7.0 mm in diameter were required to be within a tolerance of the Beard and Chuang (1987) model, where the tolerance is specified by the axis ratio oscillation amplitudes observed in the Mainz wind tunnel (Thurai et al. 2009; Szakáll et al. 2010) and the 80-m bridge experiment (Thurai and Bringi 2005). Since the axis ratio amplitude oscillation derived from the wind tunnel was not fit to drops exceeding 7.0 mm in diameter (Szakáll et al. 2010), the axis ratios observed with the 2DVD during the 80-m bridge experiment (Thurai and Bringi 2005; Thurai et al. 2007) was also employed to filter the very large drops. The resultant boundaries are similar to the shaded area of Fig. 2 in Thurai et al. (2009) and are evident as the darker regions in Fig. A1d. Since the axis ratios observed in the wind tunnel appear to reach an asymptotic value near 0.8 for raindrops exceeding about 6–7 mm in diameter (Thurai et al. 2009), this was used as an upper limit for the axis ratios of very large raindrops. The minimum axis ratio allowed for 7-mm or larger raindrops was decreased linearly with increasing diameter and was derived from a linear fit between the lower range of axis ratios observed in the wind tunnel (about 0.45) and the 80-m bridge experiment (about 0.3). The boundaries of the axis ratio filter are readily discernable in Fig. A1d, which shows that an additional 36% of the large raindrops were removed by this filter.

The size spectrum of raindrops before and after filtering the 2DVD measurements is given in Fig. A1e. Roughly 65% of the nearly 347 million objects recorded by the 2DVD were classified as raindrops as a result of this filtering process, and 25% of the objects larger than 5 mm in diameter were classified as large raindrops. The relative maximums in the unfiltered number of objects at 6-, 8-, and 10-mm diameters, which are due to calibration spheres, were removed during the filtering process (Fig. A1e).

REFERENCES

Adler, R. F., and Coauthors, 2003: The version-2 Global Precipitation Climatology Project (GPCP) monthly precipitation analysis (1979–present). *J. Hydrometeor.,* **4,** 1147–1167, doi:10.1175/1525-7541(2003)004<1147:TVGPCP>2.0.CO;2.

Atlas, D., and C. W. Ulbrich, 1977: Path- and area-integrated rainfall measurement by microwave attenuation in the 1–3 cm band. *J. Appl. Meteor.,* **16,** 1322–1331, doi:10.1175/1520-0450(1977)016<1322:PAAIRM>2.0.CO;2.

——, R. C. Srivastava, and R. S. Sekkon, 1973: Doppler radar characteristics of precipitation at vertical incidence. *Rev. Geophys.,* **11,** 1–35, doi:10.1029/RG011i001p00001.

Aydin, K., T. A. Seliga, and V. Balaji, 1986: Remote sensing of hail with a dual-linear polarization radar. *J. Climate Appl. Meteor.,* **25,** 1475–1484, doi:10.1175/1520-0450(1986)025<1475:RSOHWA>2.0.CO;2.

Balakrishnan, N., D. S. Zrnić, J. Goldhirsh, and J. Rowland, 1989: Comparison of simulated rain rates from disdrometer data employing polarimetric radar algorithms. *J. Atmos. Oceanic Technol.,* **6,** 476–486, doi:10.1175/1520-0426(1989)006<0476:COSRRF>2.0.CO;2.

Barnes, G., 2001: Severe local storms in the tropics. *Severe Convective Storms, Meteor. Monogr.,* No. 50, Amer. Meteor. Soc., 359–432.

Baumgardner, D., and A. Colpitt, 1995: Monster drops and rain gushes: Unusual precipitation phenomena in Florida marine cumulus. Preprints, *Conf. on Cloud Physics,* Dallas, TX, Amer. Meteor. Soc., 344–349.

Beard, G., P. R. Chappell, C. Ganter, G. M. Griffiths, C. P. Guard, M. A. Lander, and S. Tobin, 2013: [Regional Climate] Oceania [in "State of the Climate in 2012"]. *Bull. Amer. Meteor. Soc.,* **94** (8), S192–S197.

Beard, K. V., 1976: Terminal velocity and shape of cloud and precipitation drops aloft. *J. Atmos. Sci.,* **33,** 851–864, doi:10.1175/1520-0469(1976)033<0851:TVASOC>2.0.CO;2.

——, 1985: Simple altitude adjustments to raindrop velocities for Doppler radar analysis. *J. Atmos. Oceanic Technol.,* **2,** 468–471, doi:10.1175/1520-0426(1985)002<0468:SAATRV>2.0.CO;2.

——, and C. Chuang, 1987: A new model for the equilibrium shape of raindrops. *J. Atmos. Sci.,* **44,** 1509–1524, doi:10.1175/1520-0469(1987)044<1509:ANMFTE>2.0.CO;2.

——, D. B. Johnson, and D. Baumgardner, 1986: Aircraft observations of large raindrops in warm, shallow, convective clouds. *Geophys. Res. Lett.,* **13,** 991–994, doi:10.1029/GL013i010p00991.

Biasutti, M., S. E. Yuter, C. D. Burleyson, and A. H. Sobel, 2012: Very high resolution rainfall patterns measured by TRMM precipitation radar: Seasonal and diurnal cycles. *Climate Dyn.,* **39,** 239–258, doi:10.1007/s00382-011-1146-6.

Brandes, E. A., G. Zhang, and J. Vivekanandan, 2002: Experiments in rainfall estimation with a polarimetric radar in a subtropical environment. *J. Appl. Meteor.,* **41,** 674–685, doi:10.1175/1520-0450(2002)041<0674:EIREWA>2.0.CO;2.

——, ——, and ——, 2003: An evaluation of a drop distribution–based polarimetric radar rainfall estimator. *J. Appl. Meteor.,* **42,** 652–660, doi:10.1175/1520-0450(2003)042<0652:AEOADD>2.0.CO;2.

Bringi, V. N., and V. Chandrasekar, 2001: *Polarization Doppler Weather Radar.* Cambridge University Press, 636 pp.

——, D. A. Burrows, and S. M. Menon, 1991: Multiparameter radar and aircraft study of raindrop spectral evolution in warm-based clouds. *J. Appl. Meteor.,* **30,** 853–880, doi:10.1175/1520-0450(1991)030<0853:MRAASO>2.0.CO;2.

——, G. Huang, V. Chandrasekar, and E. Gorgucci, 2002: A methodology for estimating the parameters of a gamma raindrop size distribution model from polarimetric radar data: Application to a squall-line event from the TRMM/Brazil campaign. *J. Atmos. Oceanic Technol.,* **19,** 633–645, doi:10.1175/1520-0426(2002)019<0633:AMFETP>2.0.CO;2.

——, V. Chandrasekar, J. Hubbert, E. Gorgucci, W. L. Randeu, and M. Schoenhuber, 2003: Raindrop size distribution in different climatic regimes from disdrometer and dual-polarized radar analysis. *J. Atmos. Sci.,* **60,** 354–365, doi:10.1175/1520-0469(2003)060<0354:RSDIDC>2.0.CO;2.

——, M. Thurai, K. Nakagawa, G. J. Huang, T. Kobayahi, A. Adachi, H. Hanando, and S. Sekizawa, 2006: Rainfall estimation from C-band polarimetric radar in Okinawa, Japan: Comparisons with 2D-video disdrometer and 400 MHz wind profiler. *J. Meteor. Soc. Japan,* **84,** 705–724, doi:10.2151/jmsj.84.705.

Brunkow, D., V. N. Bringi, P. C. Kennedy, S. A. Rutledge, V. Chandrasekar, E. A. Mueller, and R. K. Bowie, 2000: A description of the CSU–CHILL National Radar Facility. *J. Atmos. Oceanic Technol.,* **17,** 1596–1608, doi:10.1175/1520-0426(2000)017<1596:ADOTCC>2.0.CO;2.

Bunkers, M. J., 2002: Vertical wind shear associated with left-moving supercells. *Wea. Forecasting,* **17,** 845–855, doi:10.1175/1520-0434(2002)017<0845:VWSAWL>2.0.CO;2.

Carey, L. D., and W. A. Petersen, 2015: Sensitivity of C-band polarimetric radar-based drop size measurements to maximum diameter. *J. Appl. Meteor. Climatol.,* doi:10.1175/JAMC-D-14-0079.1, in press.

——, S. A. Rutledge, D. A. Ahijevych, and T. D. Keenan, 2000: Correcting propagation effects in C-band polarimetric radar observations of tropical convection using differential propagation phase. *J. Appl. Meteor.,* **39,** 1405–1433, doi:10.1175/1520-0450(2000)039<1405:CPEICB>2.0.CO;2.

Cecil, D. J., and C. B. Blankenship, 2012: Toward a global climatology of severe hailstorms as estimated by satellite passive microwave imagers. *J. Climate,* **25,** 687–703, doi:10.1175/JCLI-D-11-00130.1.

Chandrasekar, V., and V. N. Bringi, 1987: Simulation of radar reflectivity and surface measurements of rainfall. *J. Atmos. Oceanic Technol.,* **4,** 464–478, doi:10.1175/1520-0426(1987)004<0464:SORRAS>2.0.CO;2.

Chang, W., 2012: Giant raindrops from sub-tropical convective precipitation system: A case study. *Extended Abstracts, Seventh European Conf. on Radar in Meteorology and Hydrology,* Toulouse, France, ERAD, 6 pp. [Available online at http://www.meteo.fr/cic/meetings/2012/ERAD/extended_abs/MIC_062_ext_abs.pdf.]

Chappell, P. R., C. Ganter, C. P. Guard, M. A. Lander, G. Macara, S. McGree, and S. Tobin, 2014: [Regional Climate] Oceania [in "State of the Climate in 2013"]. *Bull. Amer. Meteor. Soc.,* **95** (7), S204–S213.

Ducrocq, V., and Coauthors, 2014: HyMeX-SOP1: The field campaign dedicated to heavy precipitation and flash flooding in the northwestern Mediterranean. *Bull. Amer. Meteor. Soc.,* **95,** 1083–1100, doi:10.1175/BAMS-D-12-00244.1.

Frisby, E. M., and H. W. Sansom, 1967: Hail incidence in the tropics. *J. Appl. Meteor.,* **6,** 339–354, doi:10.1175/1520-0450(1967)006<0339:HIITT>2.0.CO;2.

Fritsch, J. M., R. J. Kane, and C. R. Chelius, 1986: The contribution of mesoscale convective weather systems to the warm-season precipitation in the United States. *J. Climate Appl. Meteor.,* **25,** 1333–1345, doi:10.1175/1520-0450(1986)025<1333:TCOMCW>2.0.CO;2.

Fujiwara, M., 1965: Raindrop-size distribution from individual storms. *J. Atmos. Sci.,* **22,** 585–591, doi:10.1175/1520-0469(1965)022<0585:RSDFIS>2.0.CO;2.

Fujiyoshi, Y., I. Yamamura, N. Nagumo, K. Nakagawa, K. Muramoto, and T. Shimomai, 2008: The maximum size of raindrops—Can it be a proxy of precipitation climatology? *Extended Abstracts, 15th Int. Conf. on Clouds and Precipitation,* Cancun, Mexico, International Commission on Clouds and Precipitation, P1.31. [Available online at http://cabernet.atmosfcu.unam.mx/ICCP-2008/abstracts/Program_on_line/Poster_01/Fujiyoshi_extended.pdf.]

Gorgucci, E., V. Chandrasekar, V. N. Bringi, and G. Scarchilli, 2002: Estimation of raindrop size distribution parameters from polarimetric radar measurements. *J. Atmos. Sci.,* **59,** 2373–2384, doi:10.1175/1520-0469(2002)059<2373:EORSDP>2.0.CO;2.

Gunn, R., and G. D. Kinzer, 1949: The terminal velocity of fall for water droplets in stagnant air. *J. Meteor.,* **6,** 243–248, doi:10.1175/1520-0469(1949)006<0243:TTVOFF>2.0.CO;2.

Hobbs, P. V., and A. L. Rangno, 2004: Super-large raindrops. *Geophys. Res. Lett.,* **31,** L13102, doi:10.1029/2004GL020167.

Hou, A. Y., and Coauthors, 2014: The Global Precipitation Measurement (GPM) mission. *Bull. Amer. Meteor. Soc.,* **95,** 701–722, doi:10.1175/BAMS-D-13-00164.1.

Illingworth, A. J., and I. J. Caylor, 1989: Polarization radar estimates of raindrop size spectra and rainfall rates. *J. Atmos. Oceanic Technol.,* **6,** 939–949, doi:10.1175/1520-0426(1989)006<0939:PREORS>2.0.CO;2.

——, J. W. F. Goddard, and S. M. Cherry, 1987: Polarization radar studies of precipitation development in convective storms. *Quart. J. Roy. Meteor. Soc.,* **113,** 469–489, doi:10.1002/qj.49711347604.

Jaffrain, J., and A. Berne, 2012: Influence of the subgrid variability of the raindrop size distribution on radar rainfall estimators. *J. Appl. Meteor. Climatol.,* **51,** 780–785, doi:10.1175/JAMC-D-11-0185.1.

——, A. Studzinski, and A. Berne, 2011: A network of disdrometers to quantify the small-scale variability of the raindrop size distribution. *Water Resour. Res.,* **47,** W00H06, doi:10.1029/2010WR009872.

Keenan, T. D., L. D. Carey, D. S. Zrnić, and P. T. May, 2001: Sensitivity of 5-cm wavelength polarimetric radar variables to raindrop axial ratio and drop size distribution. *J. Appl. Meteor.,* **40,** 526–545, doi:10.1175/1520-0450(2001)040<0526:SOCWPR>2.0.CO;2.

Kobayashi, T., and A. Adachi, 2001: Measurements of raindrop breakup by using UHF wind profilers. *Geophys. Res. Lett.,* **28,** 4071–4074, doi:10.1029/2001GL013254.

Kozu, T., T. Shimomai, Z. Akramin, Marzuki, Y. Shibagaki, and H. Hashiguchi, 2005: Intraseasonal variation of raindrop size distribution at Koto Tabang, West Sumatra, Indonesia. *Geophys. Res. Lett.,* **32,** L07803, doi:10.1029/2004GL022340.

Kruger, A., and W. F. Krajewski, 2002: Two-dimensional video disdrometer: A description. *J. Atmos. Oceanic Technol.,* **19,** 602–617, doi:10.1175/1520-0426(2002)019<0602:TDVDAD>2.0.CO;2.

Laws, J. O., 1941: Measurements of the fall velocity of water drops and rain drops. *Hydrology,* **22,** 709–721.

Lee, C. K., G. W. Lee, I. Zawadzki, and K. Kim, 2009: A preliminary analysis of spatial variability of raindrop size distributions during stratiform rain events. *J. Appl. Meteor. Climatol.,* **48,** 270–283, doi:10.1175/2008JAMC1877.1.

Maddox, R. A., 1980: Mesoscale convective complexes. *Bull. Amer. Meteor. Soc.,* **61,** 1374–1387, doi:10.1175/1520-0477(1980)061<1374:MCC>2.0.CO;2.

Marshall, J. S., and W. Palmer, 1948: The distribution of raindrops with size. *J. Meteor.,* **5,** 165–166, doi:10.1175/1520-0469(1948)005<0165:TDORWS>2.0.CO;2.

Maeso, J., V. N. Bringi, and V. Chandrasekar, 2005: DSD characterization and computations of expected reflectivity using data from a two-dimensional video disdrometer deployed in a tropical environment. *Proc. 2005 IEEE Int. Geoscience and Remote Sensing Symp.,* Seoul, South Korea, IEEE, 5073–5076, doi:10.1109/IGARSS.2005.1526820.

May, P. T., A. R. Jameson, T. D. Keenan, and P. E. Johnston, 2001: A comparison between polarimetric radar and wind profiler observations of precipitation in tropical showers. *J. Appl. Meteor.,* **40,** 1702–1717, doi:10.1175/1520-0450(2001)040<1702:ACBPRA>2.0.CO;2.

McFarquhar, G., 2010: Raindrop size distribution and evolution. *Rainfall, State of the Science, Geophys. Monogr.,* Vol. 191, Amer. Geophys. Union, 49–60.

Miriovsky, B. J., and Coauthors, 2004: An experimental study of small-scale variability of radar reflectivity using disdrometer observations. *J. Appl. Meteor.,* **43,** 106–118, doi:10.1175/1520-0450(2004)043<0106:AESOSV>2.0.CO;2.

Mori, S., and Coauthors, 2004: Diurnal land–sea rainfall peak migration over Sumatera Island, Indonesian Maritime Continent, observed by TRMM satellite and intensive rawinsonde soundings. *Mon. Wea. Rev.,* **132,** 2021–2039, doi:10.1175/1520-0493(2004)132<2021:DLRPMO>2.0.CO;2.

Nešpor, V., W. F. Krajewski, and A. Kruger, 2000: Wind-induced error of raindrop size distribution measurement using a two-dimensional video disdrometer. *J. Atmos. Oceanic Technol.,* **17,** 1483–1492, doi:10.1175/1520-0426(2000)017<1483:WIEORS>2.0.CO;2.

Nicholls, N., J. L. McBride, and R. J. Ormerod, 1982: On predicting the onset of the Australian wet season at Darwin. *Mon. Wea. Rev.,* **110,** 14–17, doi:10.1175/1520-0493(1982)110<0014:OPTOOT>2.0.CO;2.

Pruppacher, H. R., and K. V. Beard, 1970: A wind tunnel investigation of the internal circulation and shape of water drops falling at terminal velocity in air. *Quart. J. Roy. Meteor. Soc.,* **96,** 247–256, doi:10.1002/qj.49709640807.

Rasmussen, R. M., and A. J. Heymsfield, 1987: Melting and shedding of graupel and hail. Part I: Model physics. *J. Atmos. Sci.,* **44,** 2754–2763, doi:10.1175/1520-0469(1987)044<2754:MASOGA>2.0.CO;2.

——, V. Levizzani, and H. R. Pruppacher, 1984: A wind tunnel and theoretical study on the melting behavior of atmospheric ice particles: III. Experiment and theory for spherical ice particles of radius > 500 μm. *J. Atmos. Sci.,* **41,** 381–388, doi:10.1175/1520-0469(1984)041<0381:AWTATS>2.0.CO;2.

Rauber, R. M., K. V. Beard, and B. M. Andrews, 1991: A mechanism for giant raindrop formation in warm, shallow convective clouds. *J. Atmos. Sci.,* **48,** 1791–1797, doi:10.1175/1520-0469(1991)048<1791:AMFGRF>2.0.CO;2.

Ryzhkov, A., and D. S. Zrnić, 1995: Precipitation and attenuation measurements at a 10-cm wavelength. *J. Appl. Meteor.,* **34,** 2121–2134, doi:10.1175/1520-0450(1995)034<2120:PAAMAA>2.0.CO;2.

——, and ——, 1996: Rain in shallow and deep convection measured with a polarimetric radar. *J. Atmos. Sci.,* **53,** 2989–2995, doi:10.1175/1520-0469(1996)053<2989:RISADC>2.0.CO;2.

——, M. R. Kumjian, S. M. Ganson, and A. P. Khain, 2013: Polarimetric radar characteristics of melting hail. Part I: Theoretical simulations using spectral microphysical modeling. *J. Appl. Meteor. Climatol.,* **52,** 2849–2870, doi:10.1175/JAMC-D-13-073.1.

Sachidananda, M., and D. S. Zrnić, 1987: Rain rate estimates from differential polarization measurements. *J. Atmos. Oceanic Technol.,* **4,** 588–598, doi:10.1175/1520-0426(1987)004<0588:RREFDP>2.0.CO;2.

Schönhuber, M., G. Lammer, and W. L. Randeu, 2008: The 2D-video-distrometer. *Precipitation: Advances in Measurement, Estimation and Prediction,* S. Michaelides, Ed., Springer, 3–31.

Schuur, T. J., A. V. Ryzhkov, D. S. Zrnić, and M. Schönhuber, 2001: Drop size distributions measured by a 2D video disdrometer: Comparison with dual-polarization radar data. *J. Appl. Meteor.,* **40,** 1019–1034, doi:10.1175/1520-0450(2001)040<1019:DSDMBA>2.0.CO;2.

Smith, A. M., G. M. McFarquhar, R. M. Rauber, J. A. Grim, M. S. Timlin, B. F. Jewett, and D. P. Jorgensen, 2009: Microphysical and thermodynamic structure and evolution of the trailing stratiform regions of mesoscale convective systems during

BAMEX. Part I: Observations. *Mon. Wea. Rev.,* **137,** 1165–1185, doi:10.1175/2008MWR2504.1.

Smith, P. L., Z. Liu, and J. Joss, 1993: A study of sampling-variability effects in raindrop size observations. *J. Appl. Meteor.,* **32,** 1259–1269, doi:10.1175/1520-0450(1993)032<1259:ASOSVE>2.0.CO;2.

Stewart, R. E., J. D. Marwitz, J. C. Pace, and R. E. Carbone, 1984: Characteristics through the melting layer of stratiform clouds. *J. Atmos. Sci.,* **41,** 3227–3237, doi:10.1175/1520-0469(1984)041<3227:CTTMLO>2.0.CO;2.

Szakáll, M., K. Diehl, S. K. Mitra, and S. Borrmann, 2010: Shapes and oscillations of falling raindrops—A review. *Atmos. Res.,* **97,** 416–425, doi:10.1016/j.atmosres.2010.03.024.

Szumowski, M. J., R. M. Rauber, H. T. Ochs, and K. V. Beard, 1998: The microphysical structure and evolution of Hawaiian rainband clouds. Part II: Aircraft measurements within rainbands containing high reflectivity cores. *J. Atmos. Sci.,* **55,** 208–226, doi:10.1175/1520-0469(1998)055<0208:TMSAEO>2.0.CO;2.

Takahashi, T., K. Suzuki, M. Orita, M. Tokuno, and R. de la Mar, 1995: Videosonde observations of precipitation processes in equatorial cloud clusters. *J. Meteor. Soc. Japan,* **73,** 509–534.

Tapiador, F. J., R. Checa, and M. de Castro, 2010: An experiment to measure the spatial variability of rain drop size distribution using sixteen laser disdrometers. *Geophys. Res. Lett.,* **37,** L16803, doi:10.1029/2010GL044120.

Thurai, M., and V. N. Bringi, 2005: Drop axis ratios from a 2D video disdrometer. *J. Atmos. Oceanic Technol.,* **22,** 966–978, doi:10.1175/JTECH1767.1.

——, and ——, 2008: Polarimetric radar and advanced disdrometers. *Precipitation: Advances in Measurement, Estimation and Prediction,* S. Michaelides, Ed., Springer, 233–284.

——, G. J. Huang, V. N. Bringi, W. L. Randeu, and M. Schönhuber, 2007: Drop shapes, model comparisons, and calculations of polarimetric radar parameters in rain. *J. Atmos. Oceanic Technol.,* **24,** 1019–1032, doi:10.1175/JTECH2051.1.

——, V. N. Bringi, M. Szakáll, S. K. Mitra, K. V. Beard, and S. Borrmann, 2009: Drop shapes and axis ratio distributions: Comparison between 2D video disdrometer and wind-tunnel measurements. *J. Atmos. Oceanic Technol.,* **26,** 1427–1432, doi:10.1175/2009JTECHA1244.1.

——, ——, L. D. Carey, P. Gatlin, E. Schultz, and W. A. Petersen, 2012: Estimating the accuracy of polarimetric radar–based retrievals of drop-size distribution parameters and rain rate: An application of error variance separation using radar-derived spatial correlations. *J. Hydrometeor.,* **13,** 1066–1079, doi:10.1175/JHM-D-11-070.1.

——, ——, W. A. Petersen, and P. N. Gatlin, 2013: Drop shapes and fall speeds in rain: Two contrasting examples. *J. Appl. Meteor. Climatol.,* **52,** 2567–2581, doi:10.1175/JAMC-D-12-085.1.

——, P. N. Gatlin, V. N. Bringi, and L. D. Carey, 2014: Very large rain drops from 2D video disdrometers and concomitant polarimetric radar observations. *Extended Abstracts, Eighth European Conf. on Radar Meteorology and Hydrology (ERAD 2014),* Garmisch-Partenkirchen, Germany, Deutsches Zentrum für Luft- und Raumfahrt (German Aerospace Center), Abstract 231. [Available online at http://www.pa.op.dlr.de/erad2014/programme/ExtendedAbstracts/231_Thurai.pdf.]

Tokay, A., and P. G. Bashor, 2010: An experimental study of small-scale variability of raindrop size distribution. *J. Appl. Meteor. Climatol.,* **49,** 2348–2365, doi:10.1175/2010JAMC2269.1.

——, A. Kruger, and W. F. Krajewski, 2001: Comparison of drop size distribution measurements by impact and optical disdrometers. *J. Appl. Meteor.,* **40,** 2083–2097, doi:10.1175/1520-0450(2001)040<2083:CODSDM>2.0.CO;2.

——, ——, ——, P. A. Kucera, and A. J. P. Filho, 2002: Measurements of drop size distribution in the southwestern Amazon basin. *J. Geophys. Res.,* **107,** 8052, doi:10.1029/2001JD000355.

——, P. G. Bashor, E. Habib, and T. Kasparis, 2008: Raindrop size distribution measurements in tropical cyclones. *Mon. Wea. Rev.,* **136,** 1669–1685, doi:10.1175/2007MWR2122.1.

——, W. A. Petersen, P. Gatlin, and M. Wingo, 2013: Comparison of raindrop size distribution measurements by collocated disdrometers. *J. Atmos. Oceanic Technol.,* **30,** 1672–1690, doi:10.1175/JTECH-D-12-00163.1.

Ulbrich, C. W., 1983: Natural variations in the analytical form of the raindrop size distribution. *J. Climate Appl. Meteor.,* **22,** 1764–1775, doi:10.1175/1520-0450(1983)022<1764:NVITAF>2.0.CO;2.

——, 1985: The effects of drop size distribution truncation on rainfall integral parameters and empirical relations. *J. Climate Appl. Meteor.,* **24,** 580–590, doi:10.1175/1520-0450(1985)024<0580:TEODSD>2.0.CO;2.

——, 1992: Effects of drop-size-distribution truncation on computer simulations of dual-measurement radar methods. *J. Appl. Meteor.,* **31,** 689–699, doi:10.1175/1520-0450(1992)031<0689:EODSDT>2.0.CO;2.

——, and D. Atlas, 1998: Rainfall microphysics and radar properties: Analysis methods for drop size spectra. *J. Appl. Meteor.,* **37,** 912–923, doi:10.1175/1520-0450(1998)037<0912:RMARPA>2.0.CO;2.

Virts, K. S., J. M. Wallace, M. L. Hutchins, and R. H. Holzworth, 2013: Highlights of a new ground-based, hourly global lightning climatology. *Bull. Amer. Meteor. Soc.,* **94,** 1381–1391, doi:10.1175/BAMS-D-12-00082.1.

Williams, C., and Coauthors, 2014: Describing the shape of raindrops size distributions using uncorrelated raindrop mass spectrum parameters. *J. Appl. Meteor. Climatol.,* **53,** 1282–1296, doi:10.1175/JAMC-D-13-076.1.

Willis, P. T., and A. J. Heymsfield, 1989: Structure of the melting layer in mesoscale convective system stratiform precipitation. *J. Atmos. Sci.,* **46,** 2008–2025, doi:10.1175/1520-0469(1989)046<2008:SOTMLI>2.0.CO;2.

Zrnić, D. S., T. D. Keenan, L. D. Carey, and P. May, 2000: Sensitivity analysis of polarimetric variables at a 5-cm wavelength in rain. *J. Appl. Meteor.,* **39,** 1514–1526, doi:10.1175/1520-0450(2000)039<1514:SAOPVA>2.0.CO;2.